AGU PUBLICATIONS

Global Biogeochemical Cycles

RESEARCH ARTICLE
10.1002/2014GB004986

Key Points:
- At 1000 ppm CO_2 and modern Ω, Eocene ocean had modern DIC and low pH of 7.65
- For given Ω, [Mg] increase slightly raises and [Ca] strongly lowers buffering
- Cenozoic [Ca] decline drives evolution and stabilizes climate against CO_2 release

Supporting Information:
- Figures S1–S4 and Texts S1–S4
- Table S1
- MyAMI model source code

Correspondence to:
M. P. Hain,
m.p.hain@soton.ac.uk

Citation:
Hain, M. P., D. M. Sigman, J. A. Higgins, and G. H. Haug (2015), The effects of secular calcium and magnesium concentration changes on the thermodynamics of seawater acid/base chemistry: Implications for Eocene and Cretaceous ocean carbon chemistry and buffering, *Global Biogeochem. Cycles*, *29*, doi:10.1002/2014GB004986.

Received 17 SEP 2014
Accepted 13 MAR 2015
Accepted article online 24 MAR 2015

The effects of secular calcium and magnesium concentration changes on the thermodynamics of seawater acid/base chemistry: Implications for Eocene and Cretaceous ocean carbon chemistry and buffering

Mathis P. Hain[1], Daniel M. Sigman[2], John A. Higgins[2], and Gerald H. Haug[3]

[1]Ocean and Earth Sciences, University of Southampton, Southampton, UK, [2]Department of Geosciences, Princeton University, Princeton, New Jersey, USA, [3]Geologisches Institut, ETH, Zürich, Switzerland

Abstract Reconstructed changes in seawater calcium and magnesium concentration ($[Ca^{2+}]$, $[Mg^{2+}]$) predictably affect the ocean's acid/base and carbon chemistry. Yet inaccurate formulations of chemical equilibrium "constants" are currently in use to account for these changes. Here we develop an efficient implementation of the MIAMI Ionic Interaction Model to predict all chemical equilibrium constants required for carbon chemistry calculations under variable $[Ca^{2+}]$ and $[Mg^{2+}]$. We investigate the impact of $[Ca^{2+}]$ and $[Mg^{2+}]$ on the relationships among the ocean's pH, CO_2, dissolved inorganic carbon (DIC), saturation state of $CaCO_3$ (Ω), and buffer capacity. Increasing $[Ca^{2+}]$ and/or $[Mg^{2+}]$ enhances "ion pairing," which increases seawater buffering by increasing the concentration ratio of total to "free" (uncomplexed) carbonate ion. An increase in $[Ca^{2+}]$, however, also causes a decline in carbonate ion to maintain a given Ω, thereby overwhelming the ion pairing effect and decreasing seawater buffering. Given the reconstructions of Eocene $[Ca^{2+}]$ and $[Mg^{2+}]$ ($[Ca^{2+}]$ ~20 mM; $[Mg^{2+}]$~30 mM), Eocene seawater would have required essentially the same DIC as today to simultaneously explain a similar-to-modern Ω and the estimated Eocene atmospheric CO_2 of ~1000 ppm. During the Cretaceous, at ~4 times modern $[Ca^{2+}]$, ocean buffering would have been at a minimum. Overall, during times of high seawater $[Ca^{2+}]$, $CaCO_3$ saturation, pH, and atmospheric CO_2 were more susceptible to perturbations of the global carbon cycle. For example, given both Eocene and Cretaceous seawater $[Ca^{2+}]$ and $[Mg^{2+}]$, a doubling of atmospheric CO_2 would require less carbon addition to the ocean/atmosphere system than under modern seawater composition. Moreover, increasing seawater buffering since the Cretaceous may have been a driver of evolution by raising energetic demands of biologically controlled calcification and CO_2 concentration mechanisms that aid photosynthesis.

1. Introduction

Changes in the major ion composition modify ocean chemistry by affecting the thermodynamic activity of dissolved ions and the saturation state of dissolved salts such as calcium carbonate, $CaCO_3$. The concentrations of dissolved magnesium $[Mg^{2+}]$ and calcium $[Ca^{2+}]$ are of particular importance for the carbon cycle because these ions greatly reduce the activity of carbonate ion $[CO_3^{2-}]$ via strong anion-cation interaction [e.g., *Garrels and Thompson*, 1962; *Millero and Schreiber*, 1982] and because $[Ca^{2+}]$ is a direct factor in the saturation state of $CaCO_3$ [e.g., *Harvie et al.*, 1984]. Both $[Ca^{2+}]$ and $[Mg^{2+}]$ are reconstructed to have changed substantially in the geologic past, with evidence for almost 2 times higher $[Ca^{2+}]$ and ~40% lower $[Mg^{2+}]$ during the Eocene and up to ~4 times higher $[Ca^{2+}]$ during the Cretaceous (Figure 1) [*Lowenstein et al.*, 2001, 2003; *Dickson*, 2002, 2004; *Horita et al.*, 2002; *Lear et al.*, 2002; *Steuber and Veizer*, 2002; *Timofeeff et al.*, 2006; *Coggon et al.*, 2010; *Rausch et al.*, 2013; *Gothmann et al.*, 2015]. These large changes must be considered when attempting to reconstruct the evolution of the ocean's acid/base chemistry from observations [e.g., *Demicco et al.*, 2003; *Tyrrell and Zeebe*, 2004; *Foster et al.*, 2012], and carbon cycle models should account for the full range of aqueous chemical effects as accurately as practically possible until their impacts are fully understood.

The basic problem addressed here relates to the conventional oceanographic use of "conditional equilibrium constants" (denoted by appending an asterisk to the equilibrium constant; e.g., K^*), which define the equilibrium points of acid/base reactions in terms of "stoichiometric concentration" (square bracket notation; e.g., $[CO_3^{2-}]$)

©2015. American Geophysical Union. All Rights Reserved.

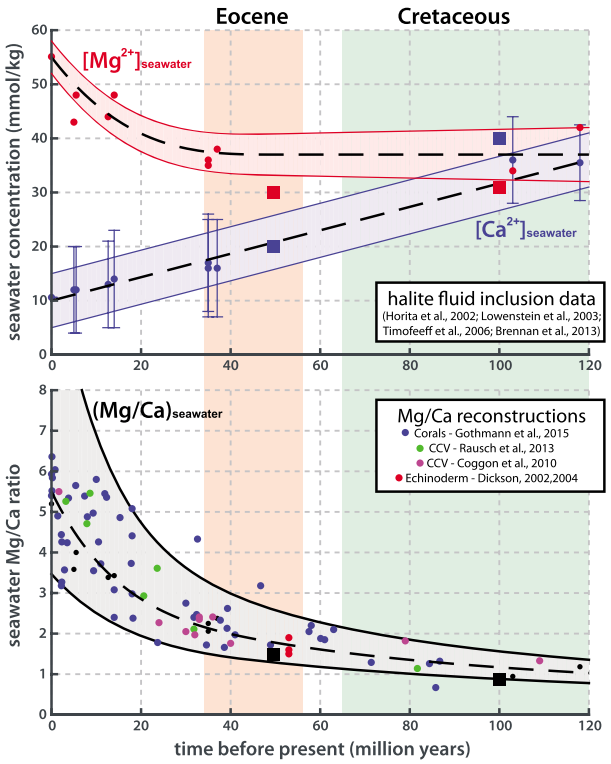

Figure 1. Reconstructed changes in (top) seawater calcium and magnesium concentration, and (bottom) seawater Mg/Ca-ratio.

as a function of temperature and salinity (*T* and *S*). This usage is different from common "thermodynamic equilibrium constants," which define the equilibrium points of acid/base reactions in terms of "activity" (curly bracket notation; e.g., $\{CO_3^{2-}\}$) as a function of temperature, ionic strength (*I*) and solution composition (*X*) (see also Table 1 for terms and symbols used in this study). To formally convert between the two systems (*K** versus *K*) requires calculating the activity coefficients for all involved chemical species, which can be done on the basis of existing experimental data sets and theory [e.g., *Pitzer*, 1973, 1991; *Harvie et al.*, 1984; *Felmy and Weare*, 1986; Greenberg and Møller, 1989; *Campbell et al.*, 1993; *Millero and Roy*, 1997; *Millero and Pierrot*, 1998]. However, due to limitations of the various existing computer models, most current efforts to simulate or reconstruct the carbon cycle of the geologic past rely on simple but inaccurate correction factors for $[Ca^{2+}]$ and $[Mg^{2+}]$ sensitivities of the thermodynamic constants (Figure 2) [i.e., *Ben-Yaakov and Goldhaber*, 1973; *Tyrrell and Zeebe*, 2004]—or they ignore seawater major ion change altogether [e.g., *Heinze and Ilyina*, 2015]. Herein, we recode the part of the MIAMI Ionic Interaction Model (Millero and Pierrot, 1998) that is required for marine acid/base chemistry in order to assist easy incorporation into carbon cycle models and other algorithmic calculations for seawater of different major ion composition than today. The Python source code of our model, MyAMI, is made available in the supporting information (MyAMI source code available at https://github.com/MathisHain/MyAMI).

Finally, as a demonstration of the importance of secular changes in seawater composition, we consider a ~50 Ma "Eocene" and a ~100 Ma "Cretaceous" scenarios, both based largely on *Demicco et al.* [2005]. Three consequences of seawater composition change are analyzed in detail: (1) the effect on the conditional equilibrium constants, (2) the effect on the CO_2-pH-DIC-Ω relationships for surface waters, and (3) changes in the ocean's buffer capacity. We find that changes in the conditional equilibrium constants are on the order of a few tens of percent, but the direct effect of elevated $[Ca^{2+}]$ on $CaCO_3$ saturation dominates the effects on speciation and equilibrium constants because it shifts the CO_2-Ω relationship toward low pH and low DIC. Our best understanding of the Eocene is that atmospheric CO_2 was as high as ~1000 ppm [e.g., *Beerling and Royer*, 2011], while reconstructions of the calcite compensation depth (CCD) require that Ω was not many fold different than in the modern ocean [e.g., *Pälike et al.*, 2012; *Ridgwell*, 2005; *Tyrrell and Zeebe*, 2004]. If reconstructions of elevated $[Ca^{2+}]$ and ~10°C higher temperatures in the Eocene are correct, then the atmospheric CO_2 and Ω constraints are attained by a DIC concentration similar to that of the modern ocean. Mainly due to elevated $[Ca^{2+}]$, seawater during the Eocene and Cretaceous must have been very poorly buffered, thereby making seawater acid/base chemistry, atmospheric CO_2, and climate more sensitive to perturbations of the global carbon cycle. The increase in the buffering capacity of the carbonate system in seawater toward the present has potentially important implications for biological systems as it would have made it progressively more energetically demanding for organisms to manipulate their internal acid/base chemistry.

2. Methods

Calculating equilibrium constants for seawater with a composition different from today requires a "Pitzer model" [e.g., *Pitzer*, 1973] to predict the activity coefficients of the chemical species involved in the marine

©2015. American Geophysical Union. All Rights Reserved.

Table 1. List of Symbols Used in the Text

	Concentration Versus Activity
$[Ca^{2+}]$, $[CO_3^{2-}]$, etc.	Square brackets denote stoichiometric concentration, including both free and complexed ion
$\{H^+\}$, $\{CO_3^{2-}\}$, etc.	Curly brackets denote the thermodynamic activity of chemical species
γ^F_{SP}	"Free ion" activity coefficient of species SP $\gamma^F_{SP} = \{SP\}/[SP]_{free}$ (equations (S4a) and (S4b))
$\gamma^T_{SP} = \gamma^F_{SP} * [SP]_{free}/\left([SP]_{free} + [SP]_{complexed}\right)$	Stoichiometric "total" activity coefficient: (equations (S5), (S6), and (S8))
	Terms Relating to Seawater
CO_2	Partial pressure of carbon dioxide in parts per million (ppm)
HCO_3^-, CO_3^{2-}, $H_2CO_3^*$	Inorganic carbon species: bicarbonate ion, carbonate ion, and carbonic acid
DIC	Dissolved inorganic carbon: sum of $[HCO_3^-]$, $[CO_3^{2-}]$, $[H_2CO_3^*]$ (3)
ALK	Alkalinity, used here including borate alkalinity: $[HCO_3^-] + 2*[CO_3^{2-}] + [B(OH)_4^-] + [OH^-] - [H^+]$
$CaCO_3$	Calcium carbonate; either calcite or aragonite polymorph
$\Omega_{calcite}$, $\Omega_{aragonite}$	Calcite and aragonite saturation state; $\Omega > 1$ is oversaturation (equations (2) and (3))
pH, pH_T	Total pH scale used throughout: $pH_T = -\log_{10}[H^+]_T = -\log_{10}([=H^+]_{free} + [HSO_4^-])$ (equation (S8))
T	Seawater temperature (for equilibrium constant calculation in Kelvin, K)
S	Seawater salinity (no units)
X	Seawater major ion composition (mole ratio relative to chloride, equation (S7b))
I	Seawater major ionic strength (mol/kg H_2O; tied to salinity after *Dickson* [2010])
	Equilibrium Constants
$K^*_0 = [H_2CO_3^*]/CO_2 = K_0\gamma^F_{CO2}/\gamma^F_{H2CO3}$	See equation (1a)—CO_2 solubility
$K^*_1 = [H^+]_T * [HCO_3^-]/[H_2CO_3^*] = K_1\gamma^F_{H2CO3}/\gamma^T_H/\gamma^F_{HCO3}$	See equation (1b)—Deprotonation of carbonic acid
$K^*_2 = [H^+]_T * [CO_3^{2-}]_T/[HCO_3^-] = K_2\gamma^F_{HCO3}/\gamma^T_H/\gamma^T_{CO3}$	See equation (1c)—Deprotonation of bicarbonate ion
$K^*_{spC} = [CO_3^{2-}]_T * [Ca^{2+}]/\Omega_{calcite} = K_{spC}/\gamma^T_{CO3}/\gamma^F_{Ca}$	See equation (1d)—Saturation of calcite
$K^*_{spA} = [CO_3^{2-}]_T * [Ca^{2+}]/\Omega_{aragonite} = K_{spA}/\gamma^T_{CO3}/\gamma^F_{Ca}$	See equation (1e)—Saturation of aragonite
$K^*_B = [H^+]_T * [B(OH)_4^-]/[H_3BO_3] = K_B\gamma^F_{H3BO3}/\gamma^T_H/\gamma^F_{B(OH)4}$	See equation (1f)—Deprotonation of boric acid
$K^*_w = [H^+]_T * [OH^-]_T = K_w/\gamma^T_H/\gamma^T_{OH}$	See equation (1g)—Autoprotolysis of water
$K^*_{HSO4} = [H^+]_T * [SO_4^{2-}]/[HSO_4^-] = K_{HSO4}\gamma^F_{HSO4}/\gamma^T_H/\gamma^F_{SO4}$	See equation (1h)—Deprotonation of bisulfate ion
	Seawater Reference Composition in mmol Per kg Solution (*Millero et al.* [2008])
$[Cl^-] = 545.8696 \times S/35$	
$[Na^+] = 468.9674 \times S/35$	
$[Mg^{2+}] = 52.7171 \times S/35$	Magnesium concentration is being explicitly changed
$[SO_4^{2-}] = 28.2352 \times S/35$	
$[Ca^{2+}] = 10.2821 \times S/35$	Calcium concentration is being explicitly changed
$[K^+] = 10.2077 \times S/35$	
$[HCO_3^-] = 1.7177 \times S/35$	
$[CO_3^{2-}] = 0.239 \times S/35$	
$[B(OH)_4^-] = 0.1008 \times S/35$	
$[Sr^{2+}] = 0.0907 \times S/35$	
$[H_2CO_3^*]$, $[H_3BO_3]$, $[H^+]$, $[OH^-]$, $[HSO_4^-]$	Neutral and minor species assume nominal concentration (pH ~8)

acid/base chemistry. There are a number of models available to carry out these calculations, e.g., (1) PHREEQC distributed by the U.S. Geological Survey [*Parkhurst*, 1995], (2) the EQL/EVP model for evaporation and mineral precipitation of brines (Risacher and Clemant, 2001), (3) commercial software such as MINEQL+, and (4) the MIAMI model [*Millero and Pierrot*, 1998]. Unfortunately, for a number of reasons none of these codes are adequate to be used for carbon cycle modeling. PHREEQC by itself is not intended for brines with ionic strength as high as seawater, and it yields inaccurate results for modern seawater composition when using the included Pitzer model package (Figure 3). EQL/EVP uses (a) outdated Pitzer coefficients for carbon species (with a nominal validity range of only 20–30°C) and (b) an integrated software design that precludes direct access to the Pitzer model part. MINEQL+ is not considered here because it is expensive, not open source, not cross platform, and invalid for ionic strength of seawater. MIAMI is the only existing code that has been successfully validated against empirical equilibrium constants of modern seawater, but it exists embedded in a spreadsheet file (D. Pierrot, personal communication, 2014) making it only appropriate for one-off calculations.

For this study, we recode the part of the MIAMI model that is relevant to the bulk acid/base chemistry of seawater. Our model, MyAMI, yields results that are in good agreement with the original MIAMI model and with the empirical equilibrium constants (see Figures S1 and S2). We note that (1) there are differences

©2015. American Geophysical Union. All Rights Reserved.

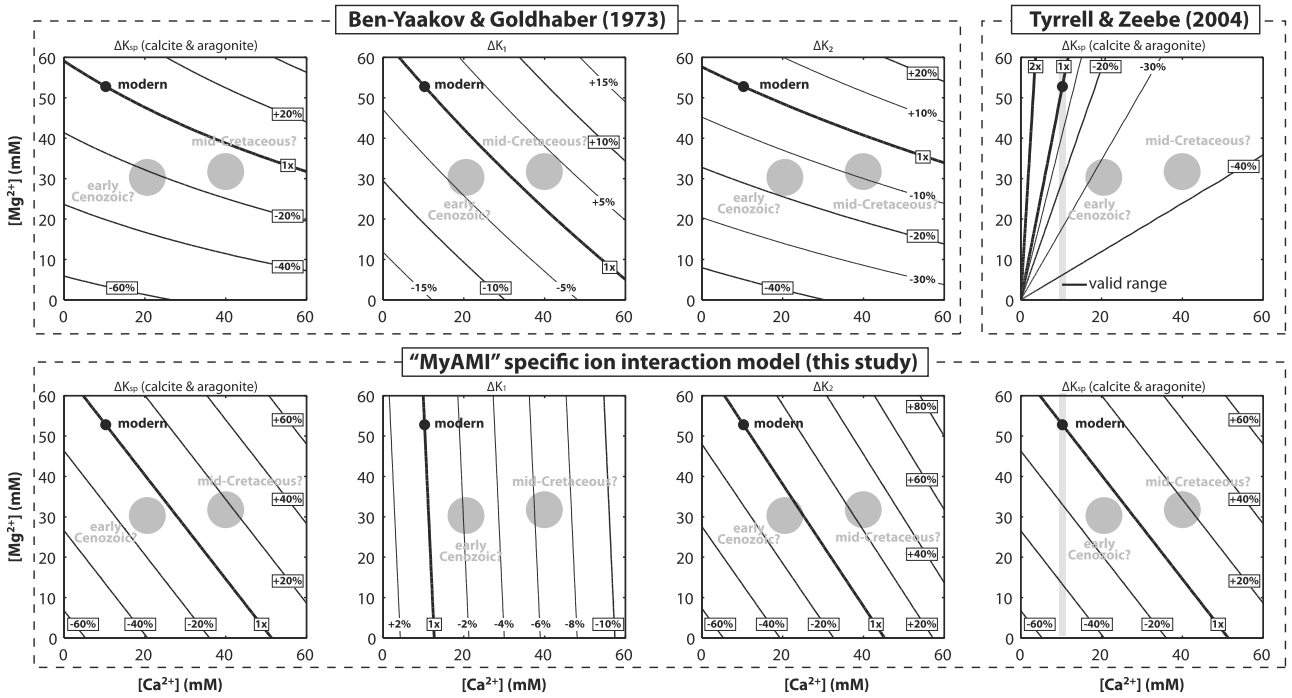

Figure 2. The equilibria of acid/base reactions as described by conditional equilibrium constants (K^*) change with the ionic composition of the solution, and in particular with changes in the concentration of the divalent cations calcium and magnesium ($[Ca^{2+}]$, $[Mg^{2+}]$). Reconstructed $[Ca^{2+}]$ and $[Mg^{2+}]$ change since the Cretaceous caused significant changes of the conditional equilibrium constants. Predicted change of equilibrium constants ($\Delta K^*/K^*_{empirical}$) in response to $[Ca^{2+}]$ and $[Mg^{2+}]$ change based on (top row) previously published corrections differ significantly from (bottom row) Pitzer-type specific ionic interaction model results. The MyAMI ion pairing model used here is a simplified version of the MIAMI model [*Millero and Pierrot*, 1998], drawing on a much larger thermodynamic database than the previous corrections. Moreover, so far corrections are available only for the equilibrium constants shown here: (K_1*) the deprotonation of carbonic acid, (K_2*) the deprotonation of bicarbonate ion, and (K_{sp}*) the solubility product of $CaCO_3$. In this study, we derive conditional equilibrium constants for the entire range of acid/base equilibria required for carbon cycle modeling (see Figures 3). All results here are for 25°C and $S = 35$.

in thermodynamic database used in MIAMI and MyAMI (see Table 2), and (2) the equilibrium constants calculated here are fully consistent with the empirical equilibrium constants because we use MyAMI only to predict the effects of changes in seawater composition (see equation (S2) in the supporting information). For additional information on the model—and for model validation—the reader is referred to the supporting information of this study and to the original description of the MIAMI model by *Millero and Pierrot* [1998]. The source code of MyAMI, in the Python programming language, is also made available online (MyAMI source code available at https://github.com/MathisHain/MyAMI).

3. Results

3.1. Equilibrium Constants

Carbon cycle modeling, and in fact every quantitative treatment of the acid/base chemistry of seawater, has either ignored the sensitivities of the equilibrium constants to seawater major ion composition or relied on simple formulations that were developed to correct for these effects [e.g., *Ben-Yaakov and Goldhaber*, 1973; *Tyrrell and Zeebe*, 2004]. By comparing to MyAMI model output, we find these simple correction factors to be inadequate (Figure 2). As pointed out by *Roberts and Tripati* [2009], the *Tyrrell and Zeebe* [2004] correction for the calcite solubility product (pK_{spC}*) agrees poorly with the MIAMI model [*Millero and Pierrot*, 1998] when considering variations in both $[Ca^{2+}]$ and $[Mg^{2+}]$. This is unsurprising because *Tyrrell and Zeebe* [2004] derive their correction based on an experimental data set where only $[Mg^{2+}]$ is manipulated [*Mucci and Morse*, 1984], to which they fit a Mg/Ca-ratio dependence. Consequently, the *Tyrrell and Zeebe* [2004] formulation agrees rather well with the MyAMI model when only $[Mg^{2+}]$ is changed at constant modern $[Ca^{2+}]$ (gray shaded vertical bar in Figure 2), but it leads to substantial error when applied to seawater with modified $[Ca^{2+}]$.

©2015. American Geophysical Union. All Rights Reserved.

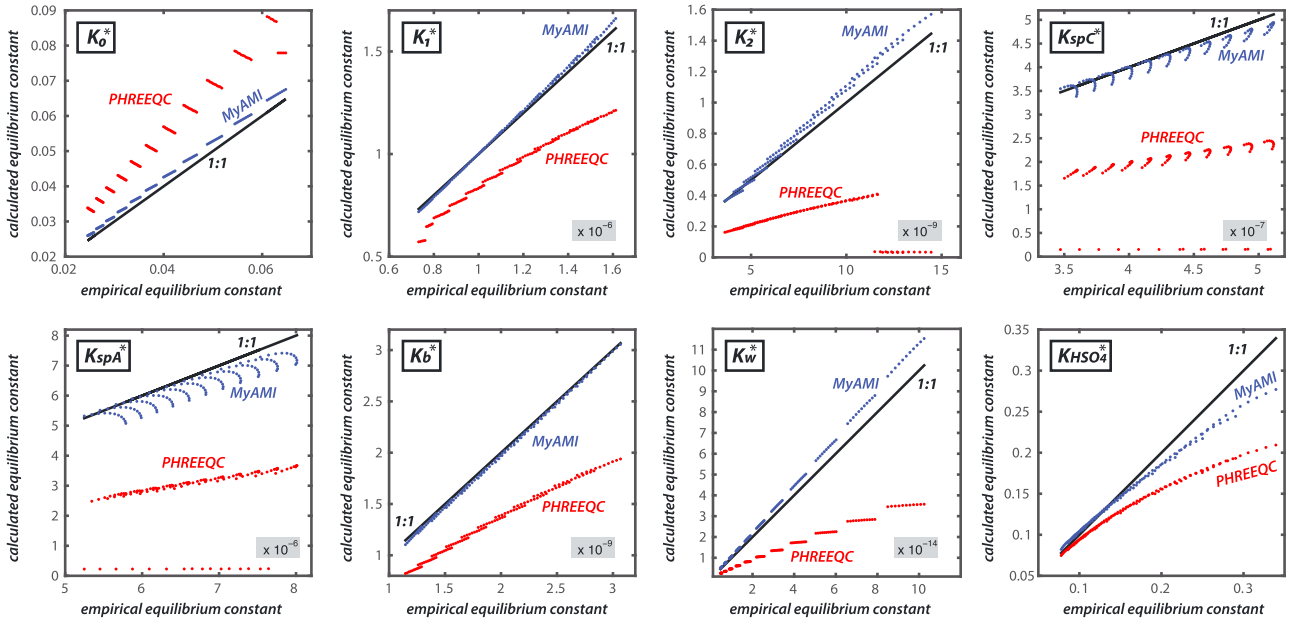

Figure 3. Assessment of model skill by comparison of predicted conditional equilibrium constants of MyAMI (blue; this study) and PHREEQC (red) [*Parkhurst*, 1995] against the empirical conditional equilibrium constants for modern seawater composition [*Weiss*, 1974; *Lueker et al.*, 2000; *Dickson et al.*, 1990a, 1990b; *Mucci*, 1983] in the range of 0–30°C and salinity of 30–40. Our MyAMI model closely tracks the "1:1" line target of perfect agreement with the empirical data. MIAMI model output (not shown) is very similar to MyAMI (see Figure S1). The equilibrium constants documented in this study are made to fully conform to empirical data by using MyAMI only to calculate the change of the equilibrium constants relative to modern seawater (according to supporting information equation (S2)).

Table 2. References for Thermodynamic Data Used in This Study[a,b,c,d,e]

	H^+	Na^+	K^+	Mg^{2+}	Ca^{2+}	Sr^{2+}	$MgOH^+$
OH^-	X	20[f]	11,12	X	15	10[g]	
Cl^-	18[f]	1[f]	1	2	1	11,13,14	15
$HCO3^-$	X	4[f]	7	10,16	15	10[g]	
$HSO4^-$	X	3[f]	15	10[f]	15	10[g]	
$B(OH)_4^-$	X	6[f]	6[f]	9[f]	9	10[g]	
CO_3^{2-}	X	4[f]	8	X	X	X	
SO_4^{2-}	X	1[f]	1	2	22[f]	10[g]	

[a]References are as follows: (1) *Møller* [1988], *Greenberg and Møller* [1989], (2) *Pabalan and Pitzer* [1987], (3) *Pierrot et al.* [1997], (4) *Peiper and Pitzer* [1982], (6) *Simonson et al.* [1988], (7) *Roy et al.* [1983], (8) *Simonson et al.* [1987a], (9) *Simonson et al.* [1987b], (10) *Millero and Pierrot* [1998], (11) *Pitzer and Mayorga* [1973], (12) *Criss and Millero* [1996], (13) *Silvester and Pitzer* [1978], (14) *Millero and Pierrot* [1998], referenced to *Criss and Millero* [1999]; (15) *Harvie et al.* [1984], (16) *Thurmond and Millero* [1982], (18) *Campbell et al.* [1993], (20) *Rai et al.* [2002], (21) *Pitzer et al.* [1985], *He and Morse* [1993], and (22) *Pitzer and Mayorga* [1974]; X denotes explicitly treated ion pairing or acid/base equilibria.

[b]References for cation-cation, anion-anion, cation-cation-anion, and anion-anion-cation Pitzer parameters are used as listed in Tables A10 and A11 of *Millero and Pierrot* [1998]; $\Theta Cl^- \text{-} CO_3^{2-}$ is corrected after *Peiper and Pitzer* [1982]; $\Theta OH^- \text{-} CO_3^{2-} = 0.1$ after *Pitzer* [1991] and *Clegg et al.* [1994].

[c]Neutral species interaction parameters for CO_2^{aq} and H_3BO_3 are taken from *He and Morse* [1993] and *Felmy and Weare* [1986].

[d]Activity coefficient for Ca-CO_3^0, Mg-CO_3^0, and Sr-CO_3^0 ion pairs is taken to be 1 following *Harvie et al.* [1984] and *He and Morse* [1993]; but see also *Millero and Schreiber* [1982].

[e]The empirical equilibrium constants are taken from (K_0*) *Weiss* [1974], (K_1* and K_2*) *Lueker et al.* [2000], (K_B*) *Dickson* [1990b], (K_{HSO4}*) *Dickson* [1990a], (K_{spC}*and K_{spA}*) *Mucci* [1983], and (K_w*) *Millero* [1995]. The thermodynamic equilibrium constants used to calculate conditional equilibrium constants are taken from (K_0 and K_1) *Plummer and Busenberg* [1982], (K_2) *Harned and Scholes* [1941] refit by *Millero* [1979], (K_B) *Owen* [1934], *Manov et al.* [1944] refit by *Millero* [1979], (K_{HSO4}) *Campbell et al.* [1993], (K_{spC} and K_{spA}) *Mucci* [1983], and (K_w) *Harned and Owen* [1958] refit by *Millero* [1979]. All conditional constants are on the total pH scale calculated using K_{HSO4}* of *Dickson* [1990a].

[f]Different value or different reference than given in *Millero and Pierrot* [1998].

[g]Equated to Ca^{2+} interaction by *Millero and Pierrot* [1998]; changes (*) carried over.

©2015. American Geophysical Union. All Rights Reserved.

In carbon cycle models, the equilibrium constants are represented by functional forms that have been used to fit the empirical data sets for modern seawater [see *Dickson et al.*, 2007; *Millero*, 1995]:

$$\ln K_0^* = p_{0,0} + \frac{p_{0,1}*100}{T} + p_{0,2}*\ln\frac{T}{100} + S*\left(p_{0,3} + \frac{p_{0,4}*T}{100} + p_{0,5}*\left(\frac{T}{100}\right)^2\right) \tag{1a}$$

$$\log_{10} K_1^* = p_{1,0} + \frac{p_{1,1}}{T} + p_{1,2}*\ln T + p_{1,3}*S + p_{1,4}*S^2 \tag{1b}$$

$$\log_{10} K_2^* = p_{2,0} + \frac{p_{2,1}}{T} + p_{2,2}*\ln T + p_{2,3}*S + p_{2,4}*S^2 \tag{1c}$$

$$\ln K_B^* = p_{B,0} + p_{B,1}*\sqrt{S} + p_{B,2}*S + \frac{1}{T}\left(p_{B,3} + p_{B,4}*\sqrt{S} + p_{B,5}*S + p_{B,6}*S^{1.5} + p_{B,7}*S^2\right) + \ln T\left(p_{B,8} + p_{B,9}*\sqrt{S} + p_{B,10}*S\right) + p_{B,11}*T*\sqrt{S} \tag{1d}$$

$$\ln K_W^* = p_{W,0} + \frac{p_{W,1}}{T} + p_{W,2}*\ln T + \sqrt{S}\left(\frac{p_{W,3}}{T} + p_{W,4} + p_{W,5}*\ln T\right) + p_{W,6}*S \tag{1e}$$

$$\log_{10} K_{spC}^* = p_{spC,0} + p_{spC,1}*T + \frac{p_{spC,2}}{T} + p_{spC,3}*\log_{10} T + \sqrt{S}\left(p_{spC,4} + p_{spC,5}*T + \frac{p_{spC,6}}{T}\right) + p_{spC,7}*S + p_{spC,8}S^{1.5} \tag{1f}$$

$$\log_{10} K_{spA}^* = p_{spA,0} + p_{spA,1}*T + \frac{p_{spA,2}}{T} + p_{spA,3}*\log_{10} T + \sqrt{S}\left(p_{spA,4} + p_{spA,5}*T + \frac{p_{spA,6}}{T}\right) + p_{spA,7}*S + p_{spA,8}S^{1.5} \tag{1g}$$

$$\ln K_{HSO4}^* = p_{HSO4,0} + \frac{p_{HSO4,1}}{T} + p_{HSO4,2}*\ln T + \sqrt{I}\left(\frac{p_{HSO4,3}}{T} + p_{HSO4,4} + p_{HSO4,5}*\ln T\right) + I\left(\frac{p_{HSO4,6}}{T} + p_{HSO4,7} + p_{HSO4,8}*\ln T\right) + \frac{p_{HSO4,9}}{T}*I^{1.5} + \frac{p_{HSO4,10}}{T}*I^2 + \ln(1 - 0.001005*S). \tag{1h}$$

These general equations explicitly represent the dependencies to changes in temperature and salinity (T, S), whereas the dependence on seawater composition (X) is implicitly encoded into the various parameters. That is, the various parameters "p" can be determined so as to fit the general equations to output from the MyAMI model at any arbitrary seawater composition (see equation (S3) in the supporting information). For later reference, Table 3 shows the parameters p for (a) modern seawater, (b) the Eocene seawater scenario, and (c) the Cretaceous scenario. A much more extensive list of tabulated parameter sets is provided in the supporting information (0 to 60 mM [Ca^{2+}] and [Mg^{2+}] range with 1 mM increments; Table S1).

3.2. Surface Ocean Chemistry in the Early Cenozoic

In the modern ocean, the well stratified surface water of the subtropical gyres is near equilibrium with respect to atmospheric CO_2 [*Takahashi et al.*, 2002] because of (a) a large surface area available for gas exchange, (b) a shallow mixed layer depth, which translates to a small volume of water to equilibrate, and (c) slow vertical exchange of water across the thermocline. These characteristics should also hold true for much of Earth history such that subtropical (low-latitude) surface water acid/base chemistry would be related to contemporaneous atmospheric CO_2 levels. To mathematically describe surface water chemistry, five parameters must be specified: temperature (T), salinity (S), major ion composition (X; at a nominal salinity of 35), and any combination of two additional parameters describing the state of seawater acid base chemistry (pH, CO_2, DIC, ALK, Ω, etc.). That is, the unique relationship between pH, CO_2, DIC, ALK, and Ω systematically depends on, and changes with, T, S and X.

Assuming equilibrium and without further approximation, the dependence of surface pH on atmospheric CO_2, surface calcite saturation Ω, T, S, and X is given by

$$\mathrm{pH} = \frac{1}{2}\left(\log\Omega - \log\left[Ca^{2+}\right] - \log(CO_2) + \left[pK_0^* + pK_1^* + pK_2^* - pK_{spC}^*\right]\right) \tag{2}$$

The aggregate "pK^*" term contains the entire T and S dependence, and it changes with seawater composition X. However, the aggregate pK^* term is quite insensitive to [Ca^{2+}] and [Mg^{2+}] changes. The formation of complexes with divalent cations has a very large effect on the activity coefficient of carbonate ion [*Garrels and Thompson*, 1962] (Equation (S1) in the supporting information), but since the activity coefficient of carbonate ion is identical for pK_2^* and pK_{spC}^* this effect is canceled by subtracting pK_{spC}^* from pK_2^*.

©2015. American Geophysical Union. All Rights Reserved.

Global Biogeochemical Cycles

10.1002/2014GB004986

Table 3. Parameters Describing the Temperature and Salinity Dependence Conditional on Modern, Eocene Scenario, and Cretaceous Scenario Seawater Major Ion Composition According to Equations (1a) to (1h)[a]

	*p*0	*p*1	*p*2	*p*3	*p*4	*p*5	*p*6	*p*7	*p*8	*p*9	*p*10	*p*11
						Modern: $[Ca^{2+}]$ = 10.2821 mM, $[Mg^{2+}]$ = 52.8171 mM						
pK_0*	−60.2409	93.4517	23.3585	0.023517	−0.023656	0.0047036	- - - -	- - - -	- - - -	- - - -	- - - -	- - - -
pK_1*	61.2172	−3633.86	−9.6777	0.011555	−0.0001152	- - - -	- - - -	- - - -	- - - -	- - - -	- - - -	- - - -
pK_2*	−25.929	−471.78	3.16967	0.01781	−0.0001122	- - - -	- - - -	- - - -	- - - -	- - - -	- - - -	- - - -
pK_B*	148.0248	137.1942	1.62142	−8966.9	−2890.53	−77.942	1.728	-0.0996	−24.4344	−25.085	−0.2474	0.053105
pK_w*	148.9652	−13847.26	−23.6521	118.67	−5.977	1.0495	−0.01615	- - - -	- - - -	- - - -	- - - -	- - - -
pK_{spC}*	−171.9065	−0.077993	2839.319	71.595	−0.77712	0.0028426	178.34	−0.07711	0.0041249	- - - -	- - - -	- - - -
pK_{spA}*	−171.945	−0.077993	2903.293	71.595	−0.068393	0.0017276	88.135	−0.10018	0.0059415	- - - -	- - - -	- - - -
pK_{SO4}*	141.328	−4276.1	−23.093	−13856	324.57	−47.986	35474	−771.54	114.723	−2698	1776	- - - -
						Eocene Scenario (~50 Ma): $[Ca^{2+}]$ = 20 mM, $[Mg^{2+}]$ = 30 mM						
pK_0*	−59.10558297	91.85983392	22.80815968	0.026034049	−0.025313942	0.004987136	- - - -	- - - -	- - - -	- - - -	- - - -	- - - -
pK_1*	62.19335659	−3669.526066	-9.834540861	0.011193361	−0.000113713	- - - -	- - - -	- - - -	- - - -	- - - -	- - - -	- - - -
pK_2*	−26.71121142	-437.8112533	3.287439691	0.017419883	−0.000110534	- - - -	- - - -	- - - -	- - - -	- - - -	- - - -	- - - -
pK_B*	156.169978	138.6678081	1.744675879	−9226.072384	−2874.822309	−82.05134674	1.444274205	-0.09130297	−25.71609713	−25.43581085	−0.264978916	0.054449827
pK_w*	146.6165292	−13701.93677	−23.34510121	105.5781367	−5.777126033	1.023014734	−0.016256003	- - - -	- - - -	- - - -	- - - -	- - - -
pK_{spC}*	−64.18088214	−0.044574948	143.2440176	27.67482884	−0.649495403	0.00263027	158.2903928	−0.077072307	0.004120361	- - - -	- - - -	- - - -
pK_{spA}*	−179.9975101	−0.081280132	3057.503031	75.03748481	−0.061276244	0.001715022	86.56805891	−0.100247518	0.005942857	- - - -	- - - -	- - - -
pK_{SO4}*	143.2910799	−4352.155483	−23.38877839	-13954.84693	326.3061964	−48.24583211	35397.10448	−771.2178916	114.6962928	-2652.692412	1765.000598	- - - -
						Cretaceous Scenario (~100 Ma): $[Ca^{2+}]$ = 40 mM, $[Mg^{2+}]$ = 32 mM						
pK_0*	−58.3877784	90.85340552	22.46019743	0.039823248	−0.034752808	0.006578522	- - - -	- - - -	- - - -	- - - -	- - - -	- - - -
pK_1*	67.18932711	−3916.913791	−10.54553663	0.011355982	-0.00011562	- - - -	- - - -	- - - -	- - - -	- - - -	- - - -	- - - -
pK_2*	−24.81329597	−523.3786264	3.002902784	0.017068822	−0.000108918	- - - -	- - - -	- - - -	- - - -	- - - -	- - - -	- - - -
pK_B*	159.3008023	136.4242881	1.902713041	−9404.24464	−2782.038919	−89.4841923	1.290414243	−0.082801324	−26.1662258	-25.07932031	-0.288321703	0.054177544
pK_w*	144.1332359	−13676.54317	−22.87294773	25.10849835	−3.843156186	0.731748246	-0.016375682	- - - -	- - - -	- - - -	- - - -	- - - -
pK_{spC}*	41.167495	−0.012195259	−2561.557454	−15.09625568	−0.443469509	0.002288422	129.8698493	−0.078205182	0.004168981	- - - -	- - - -	- - - -
pK_{spA}*	−168.5145238	−0.076650722	2834.453071	70.13642768	−0.067232499	0.001748572	89.2204672	−0.101390116	0.006035644	- - - -	- - - -	- - - -
pK_{SO4}*	144.8263358	−4407.614762	−23.62233848	−13844.49869	323.0478765	-47.74074044	35412.66387	−770.4184282	114.5696624	−2689.876025	1774.755137	- - - -

[a]The model is constrained to match the empirical equilibrium constants for modern seawater according to equation (S2) in the supporting information.

©2015. American Geophysical Union. All Rights Reserved.

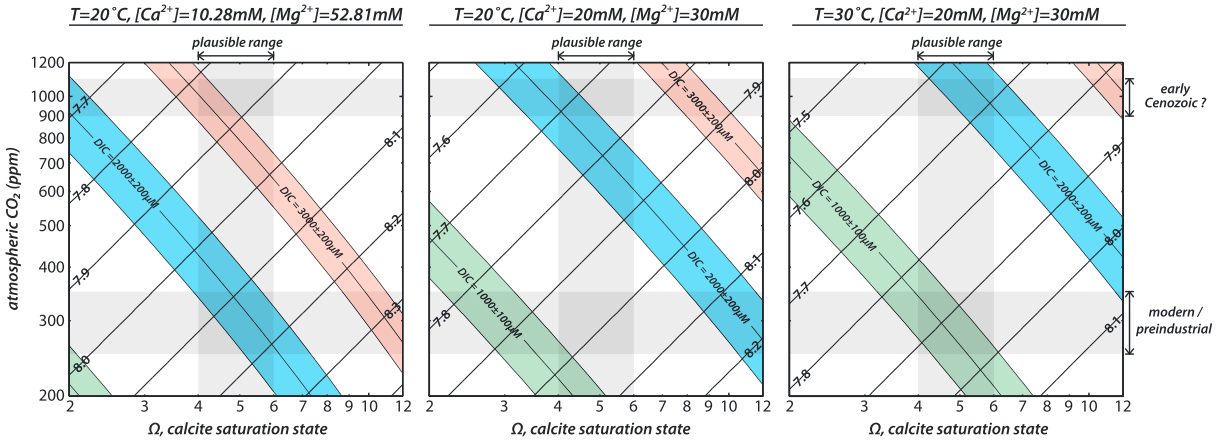

Figure 4. Thermodynamic Ω-CO_2-DIC-pH relationship for three cases of major ion composition and temperature that represent: (left) modern seawater composition at 20°C, (middle) scenario for Eocene seawater composition at 20°C, and (right) scenario for Eocene seawater composition at 30°C. Salinity (and ionic strength) is held constant at 35. Equilibrium constants are used according to equations (2) and (3). Blue, red, and green shading represents DIC ranges from 1800 to 2200 µM, 2800–3200 µM, and 900–1100 µM, respectively. Gray shading indicates modern and Eocene target CO_2 levels and the plausible rage of calcite Ω. The very mild curvature of the DIC contours results from the log(DIC/HCO_3^-) term in equation (2). Contours of ALK (not shown) would run almost parallel to DIC contours so as to yield: (1) DIC addition at constant ALK shifts the acid/base chemistry up and left in this plot (almost following DIC contours), and (2) ALK addition at constant DIC shifts the acid/base chemistry down and right in this plot (along DIC contours). Supporting information Figure S3 shows the same experiments but for the Cretaceous seawater scenario instead of the Eocene scenario.

Assuming equilibrium and without further approximation, the dependence of surface DIC on atmospheric CO_2, surface calcite saturation, *T*, *S*, and *X* is given by

$$\log[DIC] = \frac{1}{2}\left(\log\Omega - \log\left[Ca^{2+}\right] + \log CO_2 - \left[pK_0^* + pK_1^* + pK_{spC}^* - pK_2^*\right]\right) + \log\frac{[DIC]}{\left[HCO_3^-\right]}. \quad (3)$$

Note that in this expression for DIC, the aggregate *pK** term is different from the expression for pH. However, the *pK** term is again quite insensitive to $[Ca^{2+}]$ and $[Mg^{2+}]$ changes, which as above is due to the fact that pK_{spC}^* and pK_2^* are subtracted from each other so as to cancel the strong effect of the divalent metals calcium, magnesium, and strontium on the activity coefficient of carbonate ion. The last term is small because DIC ≈ HCO_3^-.

Using the above relationships that link CO_2, Ω, pH, and DIC, we consider three scenarios that illustrate the effects of seawater composition and temperature change (Figure 4), whereby the major ion change that we impose can be taken to represent early Cenozoic (Eocene) seawater (i.e., $[Ca^{2+}]$ = 20 mM and $[Mg^{2+}]$ = 30 mM; both for a nominal salinity of 35). Further, we pay particular attention to solutions of the acid/base chemistry where (a) atmospheric CO_2 is elevated to ~1000 ppm as has been proposed for the early Cenozoic [e.g., *Beerling and Royer*, 2011], and (b) the calcite saturation state Ω falls between 4 and 6, the long-term plausible range for the surface ocean since $CaCO_3$ burial came to be dominated by pelagic calcifying organisms during the mid-Mesozoic [*Ridgwell*, 2005]; for alternative argument that Ω was slightly lower prior to 40 million years ago, see *Demicco et al.* [2003].

In an ocean with modern major ion composition and temperature (Figure 4, left), there are two orthogonal ways to increase CO_2 toward the 1000 ppm target: (1) increase DIC at constant pH (roughly corresponding to an increase of DIC and ALK in a 1:1 ratio), which acts to increase Ω beyond the plausible range, and (2) decrease pH at constant DIC (i.e., a reduction in ALK), which acts to reduce Ω below plausible values. Of course, these two changes can be combined in a way that their opposing effects on Ω essentially cancel one another (yielding constant Ω of 4 to 6), and CO_2 reaches 1000 ppm due to a combination of greater DIC (>3000 µM) and lower pH (<7.95).

During the Eocene, $[Mg^{2+}]$ was lower and $[Ca^{2+}]$ was higher than in modern seawater (Figure 4, middle). As pointed out above, the strong effect of changes in divalent cation concentration essentially cancels in the aggregate *pK** terms, such that the relationships among DIC, pH, Ω, and CO_2 are approximately constant in the face of changing seawater $[Mg^{2+}]$. The concentration of $[Ca^{2+}]$, however, is a direct factor in the

©2015. American Geophysical Union. All Rights Reserved.

calculation of $CaCO_3$ saturation, and thus, it appears as a separate term in the relationships among DIC, pH, Ω, and CO_2 (equations (2) and (3)). This direct effect of calcium can be described in two equivalent ways (compare Figure 4, left and Figure 4, middle): (1) a given state of acid base chemistry (i.e., any combination of set pH, DIC, and CO_2) corresponds to a saturation state that changes proportionally with $[Ca^{2+}]$, and (2) a given coupled CO_2 and Ω target is achieved at progressively lower DIC and lower pH as $[Ca^{2+}]$ increases. If we consider explanations for elevated CO_2 during the Eocene, elevated $[Ca^{2+}]$ reduces the required DIC by lowering the pH. As for warming of subtropical surface waters during the Eocene (Figure 4, right), the most important consequences of warming are the reduction of CO_2 and $CaCO_3$ solubility (i.e., increases of pK_0^* and pK_{sp}^*), leading to two appropriate approximations: (1) warming raises CO_2 and Ω for any set DIC-pH combination, or (2) a given coupled CO_2 and Ω target is achieved at progressively higher pH and lower DIC as temperature increases.

Given the above considerations, how much error is incurred applying modern seawater equilibrium constants or the inaccurate simple correction factors that are in common use? To answer this question, it is helpful to consider equations (2) and (3) in the context of an Eocene global carbon cycle model that is spun-up to a given set level of CO_2 and Ω (e.g., via a constant CO_2 boundary condition and a steady state between riverine supply of dissolved $CaCO_3$ and seafloor $CaCO_3$ burial). Also, for this analysis we provisionally presume that our MyAMI-derived equilibrium constants are correct. First, if high Eocene $[Ca^{2+}]$ is not considered, the model will be massively wrong because $[Ca^{2+}]$ is a direct factor in determining pH and DIC. Assuming a scenario where $[Ca^{2+}]$ is doubled, simulated DIC will be √2 times higher and $[H^+]$ √2 times lower (pH 0.15 higher) than it should be. Second, given that the large changes of pK_{spC}^* and pK_2^* cancel each other the dominant change of the aggregate pK^* term in equations (2) and (3) arises from pK_1^*, which only changes modestly in our Eocene scenario (Figure 2). That is, if the carbon cycle model was using modern seawater equilibrium constants, the error in DIC and $[H^+]$ would be modest (about +2% and −5% for the Eocene and Cretaceous scenarios of Figure 2). However, in the most common case the carbon cycle model would be using the correction factors of *Ben-Yaakov and Goldhaber* [1973] and *Tyrrell and Zeebe* [2004], and thus the changes in pK_{spC}^* and pK_2^* do not cancel as they should. In this case, due to the flawed Mg/Ca-ratio assumption in the correction factor of pK_{spC}^* alone, simulated DIC would be ~17% too low and $[H^+]$ 17% too high (pH ~0.07 too low) for our Eocene seawater scenario. The magnitude of the error incurred obviously depends on the exact scenario of seawater $[Ca^{2+}]$ and $[Mg^{2+}]$ that is used, with much worse bias (about 40% for DIC and $[H^+]$) implied by the Cretaceous scenario discussed in this study.

3.3. Chemical Buffering of Seawater

The *T-S-X-*Ω-CO_2 system described above (Figure 4) is fully determined, and it fully describes the buffering of ocean chemistry against changes in DIC and ALK. Buffer factors for pH, CO_2, Ω, or any other acid/base parameter are defined as the inverse of either absolute or fractional partial derivatives in DIC or ALK [e.g., *Egleston et al.*, 2010]. Here we determine the absolute differential changes both numerically (Figure 5) and by approximate analytical solution:

$$\frac{\delta\left[CO_3^{2-}\right]}{\delta(\mathrm{DIC})} \cong \mathrm{CPF} = -\left(1+\frac{B_T}{\left[CO_3^{2-}\right]}\left(\frac{[H^+]}{K_B^*}+2+\frac{K_B^*}{[H^+]}\right)^{-1}+\frac{[H^+]^2}{K_1^*K_2^*}+\frac{K_W^*}{[H^+]\left[CO_3^{2-}\right]}+\frac{[H^+]}{\left[CO_3^{2-}\right]}\right)^{-1} \tag{4a}$$

$$\frac{\delta\left[CO_3^{2-}\right]}{\delta(\mathrm{ALK})} \cong -\mathrm{CPF} \sim \left(1+\frac{\left[B(OH)_4^-\right]}{\left[CO_3^{2-}\right]}\right)^{-1} \sim \left(1+\frac{\gamma_{CO3}^{T} B_T K_B^*}{\left\{CO_3^{2-}\right\}[H^+]}\right)^{-1} = \left(1+\frac{B_T K_B^*}{\left[HCO_3^{2-}\right]K_2^*}\right)^{-1} \tag{4b}$$

$$\frac{\delta(\mathrm{pH})}{\delta(\mathrm{ALK})} \cong \frac{1}{\left[CO_3^{2-}\right]*\ln 10}*\mathrm{CPF} \Leftrightarrow \frac{\delta(H)}{\delta(\mathrm{ALK})} \cong \frac{-[H^+]}{\left[CO_3^{2-}\right]}*\mathrm{CPF} = \frac{-\left[HCO_3^{2-}\right]K_2^*}{\left[CO_3^{2-}\right]^2}*\mathrm{CPF} \tag{4c}$$

$$\frac{\delta(CO_2)}{\delta(\mathrm{DIC})} \cong \frac{[H^+]^2}{K_0^*K_1^*K_2^*}*\mathrm{CPF} = \frac{[H_2CO_3]}{K_0^*\left[CO_3^{2-}\right]}*\mathrm{CPF} \tag{4d}$$

$$\frac{\delta(\Omega)}{\delta(\mathrm{DIC})} \cong -\frac{\left[Ca^{2+}\right]}{K_{spC}^*}*\mathrm{CPF}. \tag{4e}$$

These above formulations describe the various aspects of seawater buffering: (equations (4a) and (4b)) the sensitivity of CO_3^{2-} to incremental DIC and ALK change, (equation (4c)) the sensitivity of pH to incremental ALK

©2015. American Geophysical Union. All Rights Reserved.

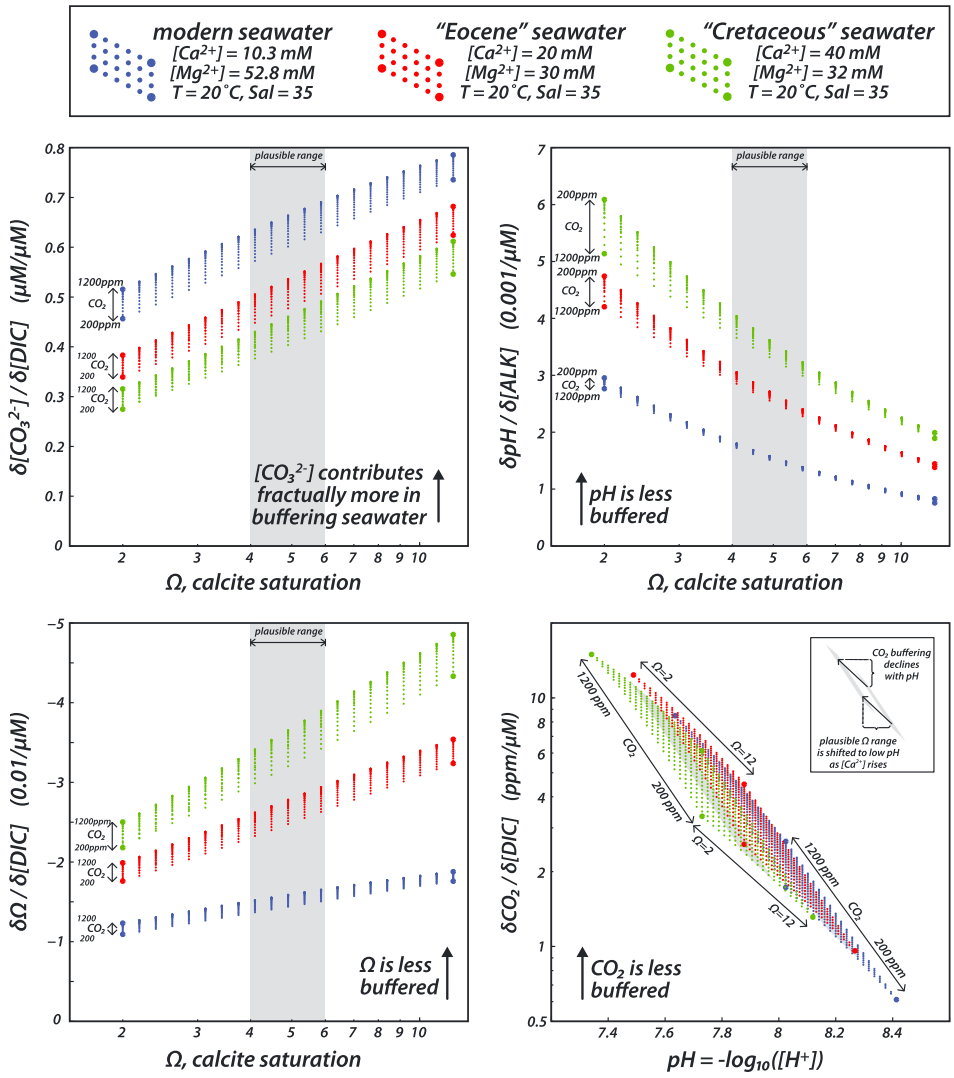

Figure 5. Sensitivity of $[CO_3^{2-}]$, pH, Ω, and CO_2 to incremental DIC and ALK change (δ/δDIC and δ/δDIC, respectively) under three cases: (blue) modern seawater major ion composition, (red) Eocene scenario major ion composition, and (green) Cretaceous scenario major ion composition. In all cases, salinity is 35 and $T = 20°C$. The points of each color span the entire solution space of $CO_2 = 200$ ppm to 1200 ppm and $\Omega = 2$ to 12. The sensitivity factors (i.e., inverse buffer factors) are numerically determined by perturbing DIC or ALK by 0.1 μM. Supporting information Figure S4 shows the same experiments but for both 20°C and 30°C, illustrating that buffering is only modestly affected by temperature (and verifying the accuracy of the approximate analytical solutions given by equation (4)).

change, (equation (4d)) the sensitivity of CO_2 to incremental DIC change, and (equation (4e)) the sensitivity of Ω to incremental DIC change. CPF, the "carbonate proton fraction," refers to the fraction of all proton transfers that is mediated by carbonate ion as opposed to the borate buffer system and the other minor contributors to seawater buffering. The approximations made in deriving these expressions are minimal, such that there is very good agreement with the numerical solutions (Figure S3). To demonstrate the effects of major ion change on seawater buffering, we consider three scenarios for seawater composition *X* (Figure 5): (blue) modern *X*, (red) Eocene *X*, and (green) Cretaceous *X*; all at $S = 35$ and $T = 20°C$. As in Figure 4, all three cases correspond to the entire solution space spanned by Ω of 2 to 12 and CO_2 in the range 200 to 1200 ppm.

Our analysis reveals three principle factors that determine seawater buffering and the change of buffering in response to changing seawater $[Ca^{2+}]$ and $[Mg^{2+}]$: (1) calcium increase in the face of constant $CaCO_3$ saturation leads to a decline in buffering because it shifts the acid/base balance of seawater toward low $[CO_3^{2-}]$ and low pH, (2) buffering is greatest when pH is near pK_1^*, pK_2^*, and pK_B^* and the conditional equilibrium constants

©2015. American Geophysical Union. All Rights Reserved.

respond to changes in seawater composition, and (3) a given perturbation of $[CO_3^{2-}]$ causes a proportionally larger change in Ω as calcium increases. With these principles in mind we describe in detail below why the change in buffering of CO_3^{2-}, pH, Ω, and CO_2 behave differently, using modern, Eocene, and Cretaceous seawater scenarios for illustration.

Carbonate ion is the main proton acceptor acting to buffer seawater against incremental addition/removal of CO_2 (δDIC) and strong acid or base (δALK), but in modern surface water about one third of the proton transfer is buffered by the equilibrium between borate and boric acid [*Frankignoulle*, 1994; *Egleston et al.*, 2010], as well as a number of numerically less important chemical species (H_2CO_3 to HCO_3^- equilibrium, H^+ to OH^- equilibrium, etc.). Thus, the sensitivity of carbonate ion to incremental DIC and ALK change is equal to the "carbonate proton fraction" (CPF in equations (4a)–(4e)), which consequently is a factor in the buffering of any other chemical species in seawater. The CPF declines (carbonate ion is mediating less of the buffering) as the ratio of borate to carbonate ion increases, which could be due to (a) greater total boron B_T, (b) lower $[CO_3^{2-}]$, or (c) higher pH at any given $[CO_3^{2-}]$ (equation (4b)). As described above, we expect high $[Ca^{2+}]$ during the Eocene and Cretaceous to drive substantially lower $[CO_3^{2-}]$ (so as to maintain relatively constant Ω) such that the CPF should have been lower and $[CO_3^{2-}]$ less sensitive to incremental DIC and ALK changes (Figure 5a). For a given CO_2, the shift toward lower $[CO_3^{2-}]$ also causes a pH decline (i.e., Figure 4; equations (2) and (3)), which counteracts some of the CPF decline. Both these effects are caused by elevated calcium in the face of relatively constant Ω.

The CPF is also affected by complex formation between carbonate ion and the divalent cations: As the summed concentration of calcium, magnesium, and strontium that increases a greater fraction of $[CO_3^{2-}]$ is complexed, the activity coefficient of carbonate ion declines (equation (S1c)), and K_2^* rises (equation (S1a), Figure 2). Thus, a rise of total divalent cation (such as in our Cretaceous scenario) increases the CPF by reducing the fraction of proton transfer that is mediated by borate ion by shifting pK_2^* down toward pK_B^*. For the Cretaceous scenario, the reduction of $[CO_3^{2-}]$ and pH in combination with the ~17% increase of K_2^* increases the borate buffer term ~2.3-fold relative to the carbonate buffer term and thus reduces the CPF from modern ~66% to Cretaceous ~45% (Figure 5a; equations (4a) and (4b)). Overall, the decline of the CPF in both Eocene and Cretaceous scenarios implies that carbonate ion contributes fractionally less to seawater buffering (borate buffering is fractionally more important), making carbonate ion less sensitive to incremental DIC and ALK perturbation. This CPF decline, however, is related to a decline in the buffering action of carbonate ion rather than an increase in the buffering action of borate, hence leaving Eocene and Cretaceous seawater less well buffered overall.

The implied poor buffering of Eocene and Cretaceous seawater becomes clear when considering the sensitivities of $[H^+]$ and pH to incremental change of DIC and ALK (Figure 5b; equation (4c)). An incremental change of carbonate ion leads to proportionally larger change of $[CO_3^{2-}]/[HCO_3^-]$ and $[H^+]$ if the initial $[CO_3^{2-}]$ is lower, such as is implied for Eocene and Cretaceous seawater. Put differently, for a given combination of CO_2 and Ω, any increase of $[Ca^{2+}]$ reduces $[CO_3^{2-}]$ so as to shift pH down and away from pK_2^* and pK_B^*, thereby making seawater less well buffered. That is, even if an incremental change of DIC or ALK causes less absolute carbonate ion change at low pH, it still causes a greater fractional change of carbonate ion. Due to this partial cancelation between the CPF term and the $[H^+]/[CO_3^{2-}]$ scaling factor, the shift in pK_2^* due to ion pairing becomes a rather significant effect on the sensitivity of $[H^+]$. The lower than modern summed concentration of divalent cations in our Eocene scenario acts to raise pK_2^* so as to further reduce the buffering of $[H^+]$ by increasing the difference between pH and pK_2^*. The reverse is true for Cretaceous scenario where summed divalent cation is greater and pK_2^* is lower than modern.

The sensitivity of saturation state (Ω) is intimately related to the sensitivity of carbonate ion to incremental DIC and ALK change (equation (4e)), such that one might surmise that Ω buffering increases as CPF declines in the Eocene and Cretaceous scenario. However, as $[Ca^{2+}]$ increases in these scenarios, a given incremental change of $[CO_3^{2-}]$ causes a proportionally larger change in Ω. That is, the effect on Ω sensitivity from the ~20% decline in CPF for the Eocene scenario is overwhelmed by ~twofold greater $[Ca^{2+}]$. Moreover, the sensitivity of Ω also scales with the activity coefficient of carbonate ion (i.e., it scales with $1/K_{spC}^*$), which rises by ~12% because the summed concentration of divalent cation is lower than modern in the Eocene scenario, such that Ω is about 1.65 times (e.g., 1.9 × calcium, 0.78 × CPF, and 1.12 × ion pairing) more sensitive

©2015. American Geophysical Union. All Rights Reserved.

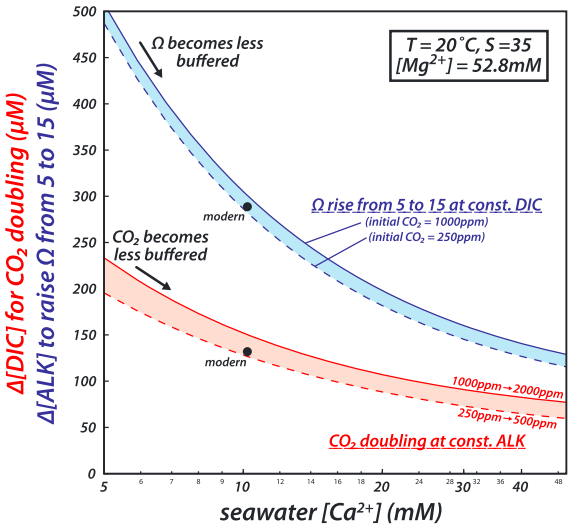

Figure 6. DIC and ALK change required to (red) double CO_2 and to (blue) raise Ω from 5 to 15 strongly decrease as seawater $[Ca^{2+}]$ concentration rises. The initial seawater is set to a CO_2 level of (dashed lines) 250 ppm or (solid lines) 1000 ppm, with Ω set to 5 in both cases.

to incremental DIC and ALK change. For the Cretaceous scenario the change is even more drastic with a 2.16 times increase in the sensitivity of Ω due to 3.8 × calcium, 0.67 × CPF, and 0.85 × ion pairing.

The buffering of CO_2 is strongly tied to both the carbonate ion to bicarbonate ion and the bicarbonate ion to carbonic acid equilibria. For this reason, the sensitivity of CO_2 is a function of the carbonic acid to carbonate ion ratio (equation (4d)). This dynamic can be described by two distinct relationships that amplify each other: (1) for a given CO_2 level $[H^+]$ increases and DIC decreases proportionally as $[CO_3^{2-}]$ declines, and (2) at a given $[CO_3^{2-}]$ concentration $[H^+]$ and DIC increase proportionally as CO_2 rises. For this reason, the sensitivity of CO_2 to incremental DIC and ALK change is very closely tied to $[H^+]$ while being essentially insensitive to DIC and with only secondary dependence on $[CO_3^{2-}]$, Ω, or CO_2.

This outcome for the buffering of CO_2 has implications for the effectiveness of carbon cycle perturbations to cause changes in atmospheric CO_2 and global climate for two related reasons. First, in a world with higher CO_2 levels, a given incremental perturbation of the carbon cycle causes a proportionally larger change in CO_2. And second, in a world with higher $[Ca^{2+}]$ (i.e., lower $[CO_3^{2-}]$) a given incremental perturbation of the carbon cycle causes a proportionally larger change in CO_2. Taking the ~3.5 × CO_2 (i.e., ~1000 ppm) and ~2 × $[Ca^{2+}]$ Eocene scenario as an example (assuming Ω = 5 and T = 20°C), a 1 μM DIC addition causes 7 ppm CO_2 change (+0.7%), which is ~5 times greater (3.5 times for CO_2, 1.9 times for $[Ca^{2+}]$, and 0.78 times for the change of CPF) than the 1.4 ppm (+0.5%) caused by the same small carbon addition to modern surface water.

Concluding the treatment of seawater buffering, we note that the sensitivities derived above are valid only for small, incremental change of DIC and ALK; and estimating the magnitude of pH, Ω, or CO_2 change by simply multiplying the sensitivity by a large change of DIC or ALK leads to substantial error. Here we solve numerically the integral of the sensitivities to calculate (a) the amount of DIC that needs to be added in order to double CO_2, and (b) the amount of ALK that needs to be added to raise Ω to some set level (Figure 6). We find that these two quantities are a strong function of seawater $[Ca^{2+}]$: Seawater becomes less well buffered as calcium is increased (at Ω = 5), and thus less DIC or ALK needs to be added to achieve any set change in seawater acid/base chemistry. As further discussed below, the two idealized experiments of Figure 6 are relevant in the context of "climate sensitivity" (i.e., equilibrium warming per CO_2 doubling likely in the range of 1.5–4.5 K per doubling; see section 10.8.2 in *Intergovernmental Panel on Climate Change* [2013] AR5) and as a driver for the evolution of calcifying organisms [e.g., *Stanley and Hardie*, 1999] and carbon concentration mechanisms [e.g., *Reinfelder*, 2011].

4. Discussion and Conclusion

4.1. Equilibrium Constants of Past Seawater

The use of empirically determined conditional equilibrium constants [*Millero*, 1995; *Dickson et al.*, 2007] associated with modern ocean major ion composition greatly simplifies calculations of seawater acid/base chemistry from field measurements and in carbon cycle models of the modern ocean because this approach implicitly accounts for "ion pairing" [*Garrels and Thompson*, 1962]. Currently available simple relationships to correct modern seawater conditional equilibrium constants for $[Ca^{2+}]$ and $[Mg^{2+}]$ changes [e.g., *Ben-Yaakov and Goldhaber*, 1973; *Tyrrell and Zeebe*, 2004] have proven inaccurate. The formulations of *Ben-Yaakov and Goldhaber* [1973] cause modest bias that could be acceptable under some circumstances. However, the pK_{spC}* correction factor

©2015. American Geophysical Union. All Rights Reserved.

derived by *Tyrrell and Zeebe* [2004] is based on a fundamentally flawed assumption (i.e., assumed Mg/Ca-ratio dependence) and insufficient thermodynamic data (only Mg^{2+} is varied), and it should therefore be avoided [see also *Roberts and Tripati*, 2009]. To be clear, the criticism of *Tyrrell and Zeebe* [2004] is limited to their treatment of pK_{spC}*, and it does not relate to the main focus of that study.

The initial impetus for this study and our "MyAMI" model was the lack of adequate equilibrium constants for carbon cycle modeling of time periods when seawater composition was different than today. The general approach taken here is not new, but we are convinced that equilibrium constants for a wide range of seawater $[Mg^{2+}]$ and $[Ca^{2+}]$ are going to be a useful resource for the field. Hence, in the supporting information, we make the source code of MyAMI available (at https://github.com/MathisHain/MyAMI), and we provide pretabulated parameters that define the temperature and salinity dependences of the conditional equilibrium constants for $[Mg^{2+}]$ and $[Ca^{2+}]$ in the range 0–60 mM (Table S1). These equilibrium constants are processed with the goal to make them suitable for inclusion in carbon cycle models: (a) in existing model code, only parameters need to be changed while the algorithms can stay the same, and (b) at modern seawater composition, the MyAMI-derived equilibrium constants conform to the empirical data sets [*Millero*, 1995; *Dickson et al.*, 2007].

4.2. Early Cenozoic Acid/Base Chemistry

Beyond its utility for carbon cycle modeling, our assessment of the thermodynamics of seawater acid/base chemistry in the face of changes in seawater $[Ca^{2+}]$ and $[Mg^{2+}]$ more generally aids in the formulation of quantitative hypotheses for the state of carbon chemistry during any given interval of Earth history. In this context, we use the Eocene period as an example for how thermodynamic considerations can be used to weigh various observations against one another. Both our choice of Eocene seawater properties ($[Ca^{2+}] = 20$ mM, $[Mg^{2+}] = 30$ mM; 10°C warming; see Figure 4c) and a rough consensus of ~1000 ppm CO_2 in early Eocene [*Beerling and Royer*, 2011] bear significant uncertainty and need not be accepted. However, if these conditions are correct, only one free parameter remains to fully determine surface ocean acid/base chemistry. The above constraints force covariation among the three parameters Ω, DIC, and pH as follows. The remaining solution space is conveniently described by two end-member scenarios: (1) near-modern surface ocean Ω and DIC at a pH of ~7.65, or (2) Ω and DIC both substantially elevated above modern values at pH substantially higher than 7.65.

No methods exist to independently reconstruct surface Ω and DIC, and available pH reconstructions for the Eocene [*Pearson and Palmer*, 1999, 2000] are vigorously debated for their underlying assumptions [e.g., *Demicco et al.*, 2003] and systematic methodological uncertainties [*Pagani et al.*, 2005]. While keeping these caveats in mind, we note that reconstructed pH for the latest Paleocene and earliest Eocene ranges between 7.6 and 7.4, while reconstructed pH mostly falls between 7.8 and 8 for the later parts of the Eocene [*Pearson and Palmer*, 2000].

The methodology of pH reconstruction based on boron isotope measurements is being continuously improved. Together with the thermodynamic considerations presented here, there is the promise that the acid/base chemistry of Eocene surface waters can be constrained with confidence in the near future. Using Pitzer parameters of *Simonson et al.* [1988] for the ion interactions of orthoborate and the divalent cations (no boric acid interactions reported), we find the boric acid dissociation constant pK_B*, which is central to the boron isotope pH proxy, to be only weakly affected by changing $[Ca^{2+}]$ and $[Mg^{2+}]$, in agreement with earlier experimental results by *Hershey et al.* [1986].

4.3. Seawater Buffering

Our results demonstrate that—mainly due to elevated $[Ca^{2+}]$ but also because of a lower than modern sum of divalent cations in the scenario—the Eocene ocean must have been less well buffered overall. The environmental and biological consequences of this change can be divided into those involving the buffering of CO_2 partial pressure and those involving the buffering of pH and Ω, as outlined below.

The buffering of CO_2 partial pressure against incremental change in DIC (and ALK) strongly depends on seawater pH, and to a lesser degree on the summed concentration of divalent cations that form complexes with carbonate ion (Figures 5b and S4; equation (4d)). Changes in ocean pH, both past and future, would then imply consequences for photosynthesizing marine organisms: in low-pH seawater, phytoplankton that rely on carbon concentrating mechanisms with active transport of DIC or ALK to improve photosynthetic efficiency [e.g., *Reinfelder*, 2011, and references therein] would have benefited from greater intracellular CO_2 increase per increment of transported chemical. Conversely, as atmospheric CO_2 declined over the Cenozoic and thus likely drove a greater need for carbon concentrating mechanisms, the secular pH rise would have necessitated

©2015. American Geophysical Union. All Rights Reserved.

greater DIC or ALK transport by carbon concentrating mechanisms to elevate phytoplankton-internal aqueous CO_2 by a given amount. This compounding of stressors was a likely driver of phytoplankton evolution toward more efficient carbon concentrating mechanisms.

The buffering of pH and Ω strongly depends on $[Ca^{2+}]$ and Ω, as well as on the summed divalent cation concentrations (~$[Mg^{2+}]$+$[Ca^{2+}]$). That is, if $[Ca^{2+}]$ was higher and Ω did not dramatically differ from its modern 4–6 range, then both Ω and pH must have been substantially less well buffered against DIC or ALK change during the Eocene (Figures 5c, 5d and S4; equations (4c) and (4e)). This finding suggests that the ocean's lysocline and calcite compensation depth (CCD) would have been more sensitive to DIC and ALK change. As a result, a given change in the global carbon cycle or the ocean's biological pump would have yielded more pronounced transient $CaCO_3$ dissolution/preservation events in the Eocene and thus shortened the timescale of imbalances in the ocean's alkalinity budget. Moreover, essentially all marine calcification is mediated or controlled by organisms that use evolved biochemical mechanisms to actively manipulate the acid/base chemistry and thus Ω at the site of calcification [e.g., *Lowenstam and Weiner*, 1989; *Gattuso et al.*, 1998; *Buitenhuis et al.*, 1999; *Iglesias-Rodriguez et al.*, 2008; *Ries et al.*, 2009; *de Nooijer et al.*, 2009; *Mackinder et al.*, 2010; *Gagnon et al.*, 2012]. In poorly buffered oceans of the past, Ω and pH are much more sensitive to incremental changes in DIC and ALK (Figure 5c, equations (4c) and (4e)), suggesting that metabolic expenditure of biologically controlled calcification should have been reduced. As a consequence, even organisms with less efficient mechanisms for increasing internal $CaCO_3$ saturation state may have been capable of hypercalcification in the poorly buffered, high-$[Ca^{2+}]$ Cretaceous ocean (blue in Figure 6). Conversely, the secular increase in seawater buffering after the mid-Cretaceous would have required more DIC and/or ALK modification to reach a given level of internal $CaCO_3$ supersaturation. This effect probably contributed to the turnover and evolution of marine organisms since that time, including the Late Cretaceous decline of rudists and the early Cenozoic rise of corals as the main reef builders. This consideration is in addition to previously discussed effects of changing seawater Mg/Ca ratio as a direct mineralogical control on the evolution of calcifying organisms [*Stanley and Hardie*, 1998, 1999; *Ries,* 2005, 2006a, 2006b; *Ries et al.*, 2006; *Stanley et al.*, 2002, 2005, 2010; *Stanley*, 2006].

Finally, the poor buffering of pre-Neogene seawater to small, incremental DIC and ALK change discussed above also translates to much larger sensitivity of pH, CO_2, and Ω to large-scale changes in the carbon cycle, such as geologic carbon release. Focusing on the sensitivity of CO_2, less carbon needs to be added to Eocene seawater in order to double its CO_2 from 1000 to 2000 ppm than is required to double CO_2 from 250 to 500 ppm under modern seawater composition (Figure 6). This finding effectively reduces the amount of geologic carbon release needed to explain the large magnitude of global warming during the Paleocene-Eocene Thermal Maximum (PETM) [e.g., *Dickens et al.*, 1995; *Pagani et al.*, 2006; *Zeebe*, 2013]. And yet, the argument by *Zeebe et al.* [2009] that a pulse of 3000 PgC is insufficient to explain the magnitude of CO_2 increase and warming still holds because they already implicitly include poor seawater buffering. It therefore appears that at least some of the carbon originated from sources other than the limited methane reservoir [e.g., *Higgins and Schrag*, 2006]. Any such geologic carbon addition would also cause greater transient shoaling of the CCD under high $[Ca^{2+}]$ with low Ω buffering (Figures 5d and 6). Beyond the PETM, the same amplified response of atmospheric CO_2 and the ocean interior's calcite saturation depth would also have applied to changes in the ocean's biological pump and other aspects of the ocean/atmosphere carbon cycle. This high sensitivity of deep ocean saturation state may help to explain the dramatic swings in lysocline depth that have been reconstructed for the early to mid-Cenozoic [*Pälike et al.*, 2012].

Poor seawater buffering and its consequences are even more extreme in the mid-Cretaceous, when seawater $[Ca^{2+}]$ was ~4 times its modern value. By the same token, seawater $[Ca^{2+}]$ today appears to be at the lowest concentration it has been in the last 100 million years, likely giving rise to the most strongly buffered seawater. In this context, we need to take careful account of changing seawater composition and buffering when comparing anthropogenic carbon release to geologic events.

Acknowledgments

The authors thank D. Pierrot, A. Mucci, F. Millero, and C. Roberts for information on the MIAMI ionic interaction model [*Millero and Pierrot*, 1998], T. Tyrrell and R. Zeebe for discussion, and R. Demicco, L. Kump, and S. Trumbore for helpful comments during review. Thermodynamic data used for the new MyAMI model are taken from the literature, with references aggregated in Table 2. Support was provided by the Charlotte Elizabeth Procter Honorific Fellowship of Princeton University (to M.P.H.), the UK NERC grant NE/K00901X/1 (to M.P.H.), the U.S. NSF grant OCE1234664 (to D.M.S.), the German DFG (Gottfried Wilhelm Leibniz Award to G.H.H), the Canadian Institute for the Advancement of Research Junior Fellowship (to J.A.H.), the Alexander von Humboldt Foundation through the Friedrich Wilhelm Bessel Award (to D.M.S.), and the John D. and Catherine T. MacArthur Foundation through its Fellows Program (to D.M.S.).

References

Beerling, D. J., and D. L. Royer (2011), Convergent Cenozoic CO_2 history, *Nat. Geosci.*, *4*, 418–420.

Ben-Yaakov, S., and M. B. Goldhaber (1973), Influence of sea-water composition on apparent constants of carbonate system, *Deep Sea Res.*, *20*(1), 87–99.

Buitenhuis, E. T., H. J. W. de Baar, and M. J. W. Veldhuis (1999), Photosynthesis and calcification by *Emiliania huxleyi* (Prymnesiophyceae) as a function of inorganic carbon species, *J. Phycol.*, *35*(5), 949–959.

©2015. American Geophysical Union. All Rights Reserved.

Campbell, D. M., F. J. Millero, R. Roy, L. Roy, M. Lawson, K. M. Vogel, and C. P. Moore (1993), The standard potential for the hydrogen-silver, silver-chloride electrode in synthetic seawater, *Mar. Chem.*, *44*(2–4), 221–233.
Clegg, S. L., J. A. Rard, and K. S. Pitzer (1994), Thermodynamic properties of 0–6 mol/kg aqueous sulfuric-acid from 273.15 to 328.15K, *J. Chem. Soc.-Faraday Trans.*, *90*(13), 1875–1894.
Coggon, R. M., D. A. H. Teagle, C. E. Smith-Duque, J. C. Alt, and M. J. Cooper (2010), Reconstructing past seawater Mg/Ca and Sr/Ca from mid-ocean ridge flank calcium carbonate veins, *Science*, *327*(5969), 1114–1117.
Criss, C. M., and F. J. Millero (1996), Modeling the heat capacities of aqueous 1–1 electrolyte solutions with Pitzer's equations, *J. Phys. Chem.*, *100*(4), 1288–1294.
Criss, C. M., and F. J. Millero (1999), Modeling heat capacities of high valence-type electrolyte solutions with Pitzer's equations, *J. Solution Chem.*, *28*(7).
de Nooijer, L. J., T. Toyofuku, and H. Kitazato (2009), Foraminifera promote calcification by elevating their intracellular pH, *Proc. Natl. Acad. Sci. U.S.A.*, *106*, 15,374–15,378.
Demicco, R. V., T. K. Lowenstein, and L. A. Hardie (2003), Atmospheric pCO_2 since 60 Ma from records of seawater pH, calcium, and primary carbonate mineralogy, *Geology*, *31*(9), 793–796.
Demicco, R. V., T. K. Lowenstein, L. A. Hardie, and R. J. Spencer (2005), Model of seawater composition for the Phanerozoic, *Geology*, *33*, 877–880.
Dickens, G. R., J. R. Oneil, D. K. Rea, and R. M. Owen (1995), Dissociation of oceanic methane hydrate as a cause of the carbon-isotope excursion at the end of the Paleocene, *Paleoceanography*, *10*(6), 965–971, doi:10.1029/95PA02087.
Dickson, A. G. (1990a), Standard potential of the reaction $AgCl(s)+1/2H_2(g)=Ag(s)+HCl(aq)$ and the standard acidity constant of the ion HSO_4 in synthetic sea-water from 273.15 to 318.15K, *J. Chem. Thermodyn.*, *22*(2), 113–127.
Dickson, A. G. (1990b), Thermodynamics of the dissociation of boric-acid in synthetic seawater from 273.15 to 318.15K, *Deep Sea Res., Part A*, *37*(5), 755–766.
Dickson, A. G. (2010), The carbon dioxide system in seawater: Equilibrium chemistry and measurements, in *Guide to Best Practices for Ocean Acidification Research and Data Reporting*, edited by V. J. F. U. Riebesell, L. Hansson, and J. P. Gattuso, pp. 17–40, European Commission, Brussels, Belgium.
Dickson, A. G., C. L. Sabine, and J. R. Christian (2007), *Guide to Best Practices for Ocean CO_2 Measurements*, 176 pp., North Pacific Marine Science Organization, Sidney, British Columbia.
Dickson, J. A. D. (2002), Fossil echinoderms as monitor of the Mg/Ca ratio of Phanerozoic oceans, *Science*, *298*(5596), 1222–1224.
Dickson, J. A. D. (2004), Echinoderm skeletal preservation: Calcite-aragonite seas and the Mg/Ca ratio of Phanerozoic oceans, *J. Sediment. Res.*, *74*(3), 355–365.
Egleston, E. S., C. L. Sabine, and F. M. M. Morel (2010), Revelle revisited: Buffer factors that quantify the response of ocean chemistry to changes in DIC and alkalinity, *Global Biogeochem. Cycles*, *24*, doi:10.1029/2008GB003407.
Felmy, A. R., and J. H. Weare (1986), The prediction of borate mineral equilibria in natural-waters—Application to Searles Lake, California, *Geochim. Cosmochim. Acta*, *50*(12), 2771–2783.
Foster, G. L., C. H. Lear, and J. W. B. Rae (2012), The evolution of pCO_2, ice volume and climate during the middle Miocene, *Earth Planet. Sci. Lett.*, *341*, 243–254.
Frankignoulle, M. (1994), A complete set of buffer factors for acid-base CO_2 system in seawater, *J. Mar. Syst.*, *5*(2), 111–118.
Gagnon, A. C., J. F. Adkins, and J. Erez (2012), Seawater transport during coral biomineralization, *Earth Planet. Sci. Lett.*, *329*, 150–161.
Garrels, R. M., and M. E. Thompson (1962), A chemical model for sea water at 25°C and one atmosphere total pressure, *Am. J. Sci.*, *260*, 57–66.
Gattuso, J. P., M. Frankignoulle, I. Bourge, S. Romaine, and R. W. Buddemeier (1998), Effect of calcium carbonate saturation of seawater on coral calcification, *Global Planet. Change*, *18*(1–2), 37–46.
Greenberg, J. P., and N. Moller (1989), The prediction of mineral solubilities in natural waters—A chemical-equilibrium model for the $Na-K-Ca-Cl-SO_4-H_2O$ system to high-concentration from 0°C to 250°C, *Geochim. Cosmochim. Acta*, *53*(10), 2503–2518.
Gothmann, A. M., J. Stolarski, J. F. Adkins, B. Schoene, K. J. Dennis, D. P. Schrag, M. Mazur, and M. L. Bender (2015), Fossil corals as an archive of secular variations in seawater chemistry since the mesozoic, *Geochim. Cosmochim. Acta*, doi:10.1016/j.gca.2015.03.018.
Harned, H. S., and B. B. Owen (1958), *The Physical Chemistry of Electrolytic Solutions*, Reinhold Publishing Corp, New York.
Harned, H. S., and S. R. Scholes (1941), The ionization constant of HCO_3^- from 0 to 50°C, *J. Am. Chem. Soc.*, *63*, 1706–1709.
Harvie, C. E., N. Moller, and J. H. Weare (1984), The prediction of mineral solubilities in natural-waters—The $Na-K-Mg-Ca-H-Cl-SO_4-OH-HCO_3-CO_3-CO_2-H_2O$ system to high ionic strengths at 25°C, *Geochim. Cosmochim. Acta*, *48*(4), 723–751.
He, S. L., and J. W. Morse (1993), The carbonic-acid system and calcite solubility in aqueous $Na-K-Ca-MgCl-SO_4$ solutions from 0 to 90°C, *Geochim. Cosmochim. Acta*, *57*(15), 3533–3554.
Heinze, M., and T. Ilyina (2015), Ocean biogeochemistry in the warm climate of the late Paleocene, *Clim Past*, *11*, 63–79, doi:10.5194/cp-11-63-2015.
Hershey, J. P., M. Fernandez, P. J. Milne, and F. J. Millero (1986), The ionization of boric-acid in NaCl, Na-Ca-Cl and Na-Mg-Cl solutions at 25°C, *Geochim. Cosmochim. Acta*, *50*(1), 143–148.
Higgins, J. A., and D. P. Schrag (2006), Beyond methane: Towards a theory for the Paleocene-Eocene Thermal Maximum, *Earth Planet. Sci. Lett.*, *245*, 523–537.
Horita, J., H. Zimmermann, and H. D. Holland (2002), Chemical evolution of seawater during the Phanerozoic: Implications from the record of marine evaporites, *Geochim. Cosmochim. Acta*, *66*(21), 3733–3756.
Iglesias-Rodriguez, M. D., et al. (2008), Phytoplankton calcification in a high-CO_2 world, *Science*, *320*, 336–340.
Intergovernmental Panel on Climate Change (2013), Detection and attribution of climate change: From global to regional, in *Climate Change 2013: The Physical Science Basis. Contribution of Working Group I to the Fifth Assessment Report of the Intergovernmental Panel on Climate Change*, edited by T. F. Stocker et al., pp. 867–952, Cambridge Univ. Press, Cambridge, U. K.
Lear, C. H., Y. Rosenthal, and N. Slowey (2002), Benthic foraminiferal Mg/Ca-paleothermometry: A revised core-top calibration, *Geochim. Cosmochim. Acta*, *66*(19), 3375–3387.
Lowenstam, H. A., and S. Weiner (1989), *On Biomineralization*, 324 pp., Oxford Univ. Press, Oxford, U. K.
Lowenstein, T. K., M. N. Timofeeff, S. T. Brennan, L. A. Hardie, and R. V. Demicco (2001), Oscillations in Phanerozoic seawater chemistry: Evidence from fluid inclusions, *Science*, *294*(5544), 1086–1088.
Lowenstein, T. K., L. A. Hardie, M. N. Timofeeff, and R. V. Demicco (2003), Secular variations in seawater chemistry and the origin of calcium chloride basinal brines, *Geology*, *31*, 857–860, doi:10.1130/G19728R.1.
Lueker, T. J., A. G. Dickson, and C. D. Keeling (2000), Ocean pCO_2 calculated from dissolved inorganic carbon, alkalinity, and equations for K_1 and K_2: validation based on laboratory measurements of CO_2 in gas and seawater at equilibrium, *Mar. Chem.*, *70*(1–3), 105–119.
Mackinder, L., G. Wheeler, D. Schroeder, U. Riebesell, and C. Brownlee (2010), Molecular mechanisms underlying calcification in coccolithophores, *Geomicrobiol. J.*, *27*, 585–595.

©2015. American Geophysical Union. All Rights Reserved.

Manov, G. G., N. J. DeLollis, and S. F. Acree (1944), Ionization constant of boric acid and the pH of certain borax-chloride buffer solutions from 0° to 60°C, *J. Res. Nat. Bur. Stds.*, *33*, 287–306.
Millero, F. J. (1979), Thermodynamics of carbonate system in seawater, *Geochim. Cosmochim. Acta*, *43*(10), 1651–1661.
Millero, F. J. (1995), Thermodynamics of the carbon-dioxide system in the oceans, *Geochim. Cosmochim. Acta*, *59*(4), 661–677.
Millero, F. J., and D. Pierrot (1998), A chemical equilibrium model for natural waters, *Aquat. Geochem.*, *4*(1), 153–199.
Millero, F. J., and D. R. Schreiber (1982), Use of the ion-pairing model to estimate activity-coefficients of the ionic components of natural-waters, *Am. J. Sci.*, *282*(9), 1508–1540.
Millero, F. J., and R. N. Roy (1997), A chemical equilibrium model for the carbonate system in natural waters, *Croat. Chem. Acta*, *70*(1), 1–38.
Millero, F. J., R. Feistel, D. G. Wright, and T. J. McDougall (2008), The composition of standard seawater and the definition of the reference-composition salinity scale, *Deep Sea Res., Part A*, *55*, 50–72.
Moller, N. (1988), The prediction of mineral solubilities in natural-waters—A chemical-equilibrium model for the Na-Ca-Cl-SO_4-H_2O system, to high-temperature and concentration, *Geochim. Cosmochim. Acta*, *52*(4), 821–837.
Mucci, A. (1983), The solubility of calcite and aragonite in seawater at various salinities, temperatures, and one atmosphere total pressure, *Am. J. Sci.*, *283*(7), 780–799.
Mucci, A., and J. W. Morse (1984), The solubility of calcite in seawater solutions of various magnesium concentration, It = 0.697M at 25°C and one atmosphere total pressure, *Geochim. Cosmochim. Acta*, *48*(4), 815–822.
Owen, B. B. (1934), The dissociation constant of boric acid from 10 to 50°C, *J. Am. Chem. Soc.*, *65*, 1695–1697.
Pabalan, R. T., and K. S. Pitzer (1987), Thermodynamics of concentrated electrolyte mixtures and the prediction of mineral solubilities to high-temperatures for mixtures in the system Na-K-Mg-Cl-SO_4-OH-H_2O, *Geochim. Cosmochim. Acta*, *51*(9), 2429–2443.
Pagani, M., D. Lemarchand, A. Spivack, and J. Gaillardet (2005), A critical evaluation of the boron isotope-pH proxy: The accuracy of ancient ocean pH estimates, *Geochim. Cosmochim. Acta*, *69*, 953–961.
Pagani, M., K. Caldeira, D. Archer, and J. C. Zachos (2006), An ancient carbon mystery, *Science*, *314*, 1556–1557.
Pälike, H., et al. (2012), A Cenozoic record of the equatorial Pacific carbonate compensation depth, *Nature*, *488*, 609–614.
Parkhurst, D. L. (1995), User's guide to PHREEQC, a computer program for speciation, reaction-path, advective-transport, and inverse geochemical calculations, U.S. Geological Survey; U.S. Geological Survey, Earth Science Information Center, Water-Resources Investigations Report 95–4227.
Pearson, P. N., and M. R. Palmer (1999), Middle Eocene seawater pH and atmospheric carbon dioxide concentrations, *Science*, *284*(5421), 1824–1826.
Pearson, P. N., and M. R. Palmer (2000), Atmospheric carbon dioxide concentrations over the past 60 million years, *Nature*, *406*(6797), 695–699.
Peiper, J. C., and K. S. Pitzer (1982), Thermodynamics of aqueous carbonate solutions including mixtures of sodium-carbonate, bicarbonate, and chloride, *J. Chem. Thermodyn.*, *14*(7), 613–638.
Pierrot, D., F. J. Millero, L. N. Roy, R. N. Roy, A. Doneski, and J. Niederschmidt (1997), The activity coefficients of HCl in HCl-Na_2SO_4 solutions from 0 to 50 degrees C and ionic strengths up to 6 molal, *J. Solution Chem.*, *26*(1), 31–45.
Pitzer, K. S. (1973), Thermodynamics of electrolytes: 1. Theoretical basis and general equations, *J. Phys. Chem.*, *77*(2), 268–277.
Pitzer, K. S. (1991), Ion interaction approach: Theory and data correlation, in *Activity Coefficients in Electrolyte Solutions*, edited by K. S. Pitzer, pp. 75–153, C.R.C. Press, Boca Raton, Fla.
Pitzer, K. S., and G. Mayorga (1973), Thermodynamics of electrolytes: 2. Activity and osmotic coefficients for strong electrolytes with one or both ions univalent, *J. Phys. Chem.*, *77*(19), 2300–2308.
Pitzer, K. S., and G. Mayorga (1974), Thermodynamics of electrolytes. III Activity and osmotic coefficients for 2–2 electrolytes, *J. Solution Chem.*, *3*(7), 539–546.
Pitzer, K. S., J. Olsen, J. M. Simonson, R. N. Roy, J. J. Gibbons, and L. Rowe (1985), Thermodynamics of aqueous magnesium and calcium bicarbonate and mixtures with chloride, *J. Chem. Eng. Data*, *30*(1), 14–17.
Plummer, L. N., and E. Busenberg (1982), The solubilities of calcite, aragonite and vaterite in CO_2-H_2O solutions between 0°C and 90°C, and an evaluation of the aqueous model for the system $CaCO_3$- CO_2-H_2O, *Geochim. Cosmochim. Acta*, *46*(6), 1011–1040.
Rai, D., N. J. Hess, L. F. Rao, Z. C. Zhang, A. R. Felmy, D. A. Moore, S. B. Clark, and G. J. Lumetta (2002), Thermodynamic model for the solubility of $Cr(OH)_3$(am) in concentrated NaOH and NaOH-$NaNO_3$ solutions, *J. Solution Chem.*, *31*(5), 343–367.
Rausch, S., F. Boehm, W. Bach, A. Kluegel, and A. Eisenhauer (2013), Calcium carbonate veins in ocean crust record a threefold increase of seawater Mg/Ca in the past 30 million years, *Earth Planet. Sci. Lett.*, *362*, 215–224.
Reinfelder, J. R. (2011), Carbon concentrating mechanisms in eukaryotic marine phytoplankton, *Annu. Rev. Mar. Sci.*, *3*, 291–315.
Ridgwell, A. (2005), A mid Mesozoic revolution in the regulation of ocean chemistry, *Mar. Geol.*, *217*, 339–357.
Ries, J. B. (2005), Aragonite production in calcite seas: Effect of seawater Mg/Ca ratio on the calcification and growth of the calcareous alga *Penicillus capitatus*, *Paleobiology*, *31*, 445–458.
Ries, J. B. (2006a), Mg fractionation in crustose coralline algae: Geochemical, biological, and sedimentological implications of secular variation in the Mg/Ca ratio of seawater, *Geochim. Cosmochim. Acta*, *70*, 891–900.
Ries, J. B. (2006b), Aragonitic algae in calcite seas: Effect of seawater Mg/Ca ratio on algal sediment production, *J. Sediment. Res.*, *76*, 515–523.
Ries, J. B., S. M. Stanley, and L. A. Hardie (2006), Scleractinian corals produce calcite, and grow more slowly, in artificial Cretaceous seawater, *Geology*, *34*, 525–528.
Ries, J. B., A. L. Cohen, and D. C. McCorkle (2009), Marine calcifiers exhibit mixed responses to CO_2-induced ocean acidification, *Geology*, *37*, 1131–1134.
Risacher, F., and A. Clemant (2001), A computer program for the simulation of evaporation of natural waters to high concentration, *Comput. Geosci.*, *27*(2), 191–201.
Roberts, C. D., and A. K. Tripati (2009), Modeled reconstructions of the oceanic carbonate system for different histories of atmospheric carbon dioxide during the last 20 Ma, *Global Biogeochem. Cycles*, *23*, doi:10.1029/2008GB003310.
Roy, R. N., J. J. Gibbons, M. D. Wood, R. W. Williams, J. C. Peiper, and K. S. Pitzer (1983), The 1st ionization of carbonic-acid in aqueous-solutions of KCl including the activity-coefficients of potassium bicarbonate, *J. Chem. Thermodyn.*, *15*(1), 37–47.
Silvester, L. F., and K. S. Pitzer (1978), Thermodynamics of electrolytes. 10 Enthalpy and effect of temperature on activity-coefficients, *J. Solution Chem.*, *7*(5), 327–337.
Simonson, J. M., R. N. Roy, and J. J. Gibbons (1987a), Thermodynamics of aqueous mixed potassium carbonate, bicarbonate, and chloride solutions to 368 K, *J. Chem. Eng. Data*, *32*(1), 41–45.
Simonson, J. M., R. N. Roy, L. N. Roy, and D. A. Johnson (1987b), The thermodynamics of aqueous borate solutions. 1 Mixtures of boric-acid with sodium or potassium borate and chloride, *J. Solution Chem.*, *16*(10), 791–803.
Simonson, J. M., R. N. Roy, D. Mrad, P. Lord, L. N. Roy, and D. A. Johnson (1988), There thermodynamics of aqueous borate solutions. 2 Mixtures of boric-acid with calcium or magnesium borate and chloride, *J. Solution Chem.*, *17*(5), 435–446.

©2015. American Geophysical Union. All Rights Reserved.

Stanley, S. M. (2006), Influence of seawater chemistry on biomineralization throughout Phanerozoic time: Paleontological and experimental evidence, *Palaeogeogr. Palaeoclimatol. Palaeoecol.*, *232*, 214–236.
Stanley, S. M., and L. A. Hardie (1998), Secular oscillations in the carbonate mineralogy of reef-building and sediment-producing organisms driven by tectonically forced shifts in seawater chemistry, *Palaeogeogr. Palaeoclimatol. Palaeoecol.*, *144*(1–2), 3–19.
Stanley, S. M., and L. A. Hardie (1999), Hypercalcification: Paleontology links plate tectonics and geochemistry to sedimentology, *Geol. Soc. Am. Bull.*, *9*(2), 1–7.
Stanley, S. M., J. B. Ries, and L. A. Hardie (2002), Low-magnesium calcite produced by coralline algae in seawater of Late Cretaceous composition, *Proc. Natl. Acad. Sci. U.S.A.*, *99*(24), 15,323–15,326.
Stanley, S. M., J. B. Ries, and L. A. Hardie (2005), Seawater chemistry, coccolithophore population growth, and the origin of Cretaceous chalk, *Geology*, *33*, 593–596.
Stanley, S. M., J. B. Ries, and L. A. Hardie (2010), Increased production of calcite and slower growth for the major sediment-producing alga Halimeda as the Mg/Ca ratio of seawater is lowered to a "calcite sea" level, *J. Sediment. Res.*, *80*, 6–16.
Steuber, T., and A. Veizer (2002), Phanerozoic record of plate tectonic control of seawater chemistry and carbonate sedimentation, *Geology*, *30*(12), 1123–1126.
Takahashi, T., et al. (2002), Global sea-air CO_2 flux based on climatological surface ocean pCO_2, and seasonal biological and temperature effects, *Deep Sea Res., Part II*, *49*(9–10), 1601–1622.
Thurmond, V., and F. J. Millero (1982), Ionization of carbonic-acid in sodium-chloride solutions at 25°C, *J. Solution Chem.*, *11*(7), 447–456.
Timofeeff, M. N., T. K. Lowenstein, M. A. da Silva, and N. B. Harris (2006), Secular variation in the major-ion chemistry of seawater: Evidence from fluid inclusions in Cretaceous halites, *Geochim. Cosmochim. Acta*, *70*, 1977–1994.
Tyrrell, T., and R. E. Zeebe (2004), History of carbonate ion concentration over the last 100 million years, *Geochim. Cosmochim. Acta*, *68*(17), 3521–3530.
Weiss, R. F. (1974), Carbon dioxide in water and seawater: The solubility of a non-ideal gas, *Mar. Chem.*, *2*, 203–215.
Zeebe, R. E. (2013), What caused the long duration of the Paleocene-Eocene Thermal Maximum?, *Paleoceanography*, *28*, 440–452, doi:10.1002/palo.20039.
Zeebe, R. E., J. C. Zachos, and G. R. Dickens (2009), Carbon dioxide forcing alone insufficient to explain Palaeocene–Eocene Thermal Maximum warming, *Nat. Geosci.*, *2*, 576–580, doi:10.1038/ngeo578.

©2015. American Geophysical Union. All Rights Reserved.

Global Biogeochemical Cycles

Supporting Information for

The effects of secular calcium and magnesium concentration changes on the thermodynamics of seawater acid/base chemistry: Implications for Eocene and Cretaceous ocean carbon chemistry and buffering

Mathis P. Hain[1*], Daniel M. Sigman[2], John A. Higgins[2], and Gerald H. Haug[3]

[1] Ocean and Earth Sciences, University of Southampton, Southampton SO143ZH, UK, [2] Department of Geosciences, Princeton University, [3] Geologisches Institut, ETH Zürich, [*] Corresponding author address: Dr. Mathis Hain, Ocean and Earth Sciences, University of Southampton, Southampton SO143ZH, UK; www.mathis-hain.net

Contents of this file

Additional Supporting Information (Files uploaded separately)

Introduction

This Supporting Information document describes a number of aspects relating to our new MyAMI model: (S1) the chemical background, (S2) the methodology and equations, (S3) differences to the MIAMI model by Millero and Pierrot (1998), and (S4) validation of our MyAMI model relative to MIAMI and empirical conditional equilibrium constants of modern seawater.

Text S1.

General method and terminology

The conversion between "conditional equilibrium constants" (K*; with asterix) used in Oceanography and common "thermodynamic equilibrium constants" (K; no asterix) is based on the "activity coefficients" (γ^T) of the chemical species involved in the equilibrium reactions (eq. S1a; see also Table 1 for list of symbols and terms). There are two reasons why the activity of a given chemical species (e.g., CO_3^{2-}) is different from its "stoichiometric" concentration: (1)

the electrostatic ion-ion interactions in electrolyte solutions typically reduce the activity of a given species below its "free" concentration (eq. S1b; Debye and Hückel, 1923; Pitzer, 1991), and (2) some ions form strong bonds with each other (i.e., complex formation or "ion pairing"; Garrels and Thompson, 1962) such that only a fraction of that species can be said to be "free" (eq. S1c). Equation S1 illustrates these relationships with the example of the bicarbonate ion to carbonate ion acid/base equilibrium (eq. S1a), the activity of free carbonate ion (eq. S1b), and carbonate ion complex formation (eq. S1c):

$$\boldsymbol{K_2^*|_X = K_2 * \frac{\gamma_{HCO3}^T}{\gamma_H^T * \gamma_{CO3}^T}} \quad \text{(eq. S1a)}$$

$$\boldsymbol{\gamma_{CO3}^F = \frac{\{CO_3^{2-}\}}{[CO_3^{2-}]_{free}}} \quad \text{(eq. S1b)}$$

$$\boldsymbol{\gamma_{CO3}^T = \frac{[CO_3^{2-}]_{free}}{[CO_3^{2-}]_{free} + [CO_3^{2-}]_{complexed}} * \gamma_{CO3}^F} \quad \text{(eq. S1c)}$$

In this example at modern seawater composition, K_2* is ~20x larger than K_2 mainly because only ~10% of the carbonate ion is "free" as opposed to the other ~90% that are bound up in "ion pairs" with the divalent cations calcium, magnesium, and strontium. Further, this example clarifies that (a) all activity coefficients change with seawater composition, and (b) conditional equilibrium constants (e.g., K_2*) are only valid for (i.e., conditional on) a specified seawater composition.

Text S2.

Adopting the MIAMI model

For modern seawater any calculation of marine acid/base and carbon chemistry is based on empirically determined conditional equilibrium constants (e.g., Millero, 1995; Dickson et al., 2007). These empirical formulations encapsulate the temperature and salinity dependence of the equilibrium constants but are conditional on modern seawater composition, and thus they are not valid for geologic times when seawater composition differed from the modern ocean. The state-of-the-art in predicting the activity coefficients (and thus conditional equilibrium constants) for seawater of arbitrary composition is encoded in the MIAMI Ionic Interaction Model by Millero and Pierrot (1998; hereafter MP98). Here we re-implement MIAMI in simplified form to make its output suitable for systematic use in carbon chemistry calculations and modeling. To avoid confusion and to highlight that our model is based on MP98 we make the source code and tabulated model output available under the name "MyAMI."

There are two main problems that prevent the original MIAMI model from being directly adopted. First, conditional equilibrium constants for modern seawater composition predicted by the MIAMI model are in reasonably good agreement with empirically determined constants, but switching between these sets of empirical and predicted equilibrium constants will nevertheless result in spurious offsets (Figure S2). We overcome this problem by using the MIAMI model to only predict the change of the equilibrium constants relative to a fixed reference defined by the empirical equilibrium constants:

$$pK^*_{predicted}|_{(T,S,X)} = pK^*_{empirical}(T,S)|_{X_0} + \Delta pK^*_{MyAMI}|_{(T,S,X)} \quad \text{(eq. S2a)}$$

$$\Delta pK^*_{MyAMI}|_{(T,S,X)} = pK^*_{MyAMI}(T,S,X) - pK^*_{MyAMI}(T,S,X_0) \quad \text{(eq. S2b)}$$

In this notation pK* refers to the negative decimal logarithm of the equilibrium constant K*, and T, S and X refer to temperature, salinity and seawater composition (i.e., the relative proportion of chemical constituents; X_0 is modern seawater composition). As per convention, the appended asterix signifies that the constants are conditional on composition of the solution.

The second problem stems from the fact that in many cases equilibrium constants need to be recalculated billions of times to solve for the carbon chemistry in carbon cycle models, such that the direct use of the computationally inefficient MIAMI model is implausible. We overcome this problem by predicting equilibrium constants over a wide range of temperatures (0-40˚C in 21 steps of 2˚C) and salinities (30-40 in 21 steps of 0.5) and using a least square optimization algorithm to fit the same parameters that are used to describe the empirical equilibrium constants (e.g., Millero, 1995; Dickson et al., 2007; see also Equation S9 below). That is, instead of a single calculation to predict the equilibrium constants at a given T, S and X, we use the MyAMI model 21x21=441 times to predict the equilibrium constants conditional on X as a function of T and S:

$$X \xrightarrow[MIAMI]{} pK^*_{predicted}|_{(T,S,X)} \xrightarrow[least\ square]{} pK^*_{predicted}(T,S)|_X \quad \text{(eq. S3)}$$

Text S3.

Differences to MP98 MIAMI model

Our code mainly follows the detailed description of the MIAMI model by MP98. For brevity we limit the description below to the ways in which our implementation differs from MP98.

As a first point of differences, while MP98 MIAMI calculates activity coefficients for a extensive list of chemical species, MyAMI only considers the following subset: Na^+, Cl^-, Mg^{2+}, SO_4^{2-}, HSO_4^- Ca^{2+}, Sr^{2+}, K^+, $MgOH^+$, $B(OH)_4^-$, H_3BO_3, H_2CO_3, HCO_3^-, CO_3^{2-}, H^+, and OH^-. These species were chosen so that the key equilibrium constants for seawater acid/base chemistry can be predicted: solubility of CO_2 (pK_0*), deprotonation of carbonic acid (pK_1*), deprotonation of bicarbonate ion (pK_2*), equilibrium between boric acid and borate (pK_B*), deprotonation of bisulfate (pK_{HSO4}*), autoprotolysis of water (pK_W*), and the solubility product of the $CaCO_3$ polymorphs calcite and aragonite (pK_{spC}*, pK_{spA}*).

Furthermore, we use a truncated form of the general Pitzer equation (Pitzer, 1973, 1991; Millero and Pierrot, 1998):

$$\ln \gamma_M^F = \text{D.H.} + Z^2R + ZS + 2\sum_a m_a (B_{Ma} + EC_{Ma}) + \sum_c m_c (2\Theta_{Mc} + \sum_a m_a \Psi_{Mca}) + \sum_a \sum_{a'} m_a m_{a'} \Psi_{Maa'} \quad \text{(eq. S4a)}$$

$$\ln \gamma_X^F = \text{D.H.} + Z^2R + ZS + 2\sum_c m_c (B_{cX} + EC_{cX}) + \sum_a m_a (2\Theta_{Xa} + \sum_c m_c \Psi_{Xac}) + \sum_c \sum_{c'} m_c m_{c'} \Psi_{Mcc'} \quad \text{(eq. S4b)}$$

where D.H. is related to the Debye-Hückel limiting law and the B, C, Θ and Ψ parameters are related to the binary and ternary interaction between the cations M, c and c', the anions X, a

and a'. Empirically determined values for these parameters are available for most major ions in seawater over a wide range of temperature (see Table 2 for the parameters used here). The terms Z^2R and ZS relate to the ionic media. Unlike MP98, we have truncated the higher-order electrostatic terms, as they are relevant only in brines with much higher ionic strength and do not substantially affect ordinary seawater.

In coding MyAMI, in some cases, parameter values characterizing the various ion-ion interactions differ from those tabulated by MP98 (Table 2). We point out that in some of these cases we refer to the same original data source, such that the difference may be the trivial result of a typographical error in MP98's aggregation of Pitzer coefficients.

As in MP98, complexation of Ca-CO_3, Mg-CO_3, Sr-CO_3 and Mg-OH are calculated explicitly via:

$$\gamma_{CO3}^{T} = \gamma_{CO3}^{F} \Big/ \left(1 + \frac{[Mg^{2+}]}{K^{*}_{Mg-CO3}} + \frac{[Ca^{2+}]}{K^{*}_{Ca-CO3}} + \frac{[Sr^{2+}]}{K^{*}_{Sr-CO3}}\right) \quad \text{(eq. S5)}$$

$$\gamma_{OH}^{T} = \gamma_{OH}^{F} \Big/ \left(1 + \frac{[Mg^{2+}]}{K^{*}_{Mg-OH}}\right) \quad \text{(eq. S6)}$$

The terms γ^T and γ^F refer to the total (stoichiometric) activity coefficient and the activity coefficient of free (uncomplexed) ion, respectively (Equation S1). We calculate the conditional stability constants (K*) based on ion pair formation constants of Millero and Roy (1997), using free ion activity coefficients from the specific ion interaction model (i.e., for CO_3^{2-}, OH^-, the divalent cations, Mg-OH^+), and we assume an activity of 1 for the neutral metal-CO_3 ion pairs (see Millero and Schreiber (1982) and discussion by He and Morse (1993); but see also Reardon and Langmuir (1976)). The underlying assumption for the neutral metal-CO_3 ion pairs is not clearly specified in MP98.

For practical reasons we work under the premise of set modern seawater relationships among "Practical Salinity Scale" salinity (UNESCO, 1981), ionic strength (I), and chlorinity (Dickson, 2010):

$$I = \frac{19.924 * S}{1000 - 1.005 * S} \quad \text{(eq. S7a)}$$

$$Cl\ [mol\ kg^{-1}] = 0.5458696 * \frac{S}{35} \quad \text{(eq. S7b)}$$

The concentrations of the other seawater constituents (except for $[Ca^{2+}]$ and $[Mg^{2+}]$, which are deliberately varied) are tied to their proportional abundance relative to chloride as defined by the seawater reference composition (Millero et al., 2008). That is, we prefer to ignore the small effects of imposed $[Ca^{2+}]$ and $[Mg^{2+}]$ change on the relationship between salinity and ionic strength (S and I) because we believe that ocean S and I are dominantly controlled through net precipitation/dissolution of rock salt (NaCl), and in absence of evidence that S and I changed in the past we choose to assume that they remained constant.

Finally, in keeping with convention, we derive conditional equilibrium constants relative to the total pH scale (pH_T) via an adjustment to the activity coefficient of H^+ to account for the protonation of sulphate ion (Dickson, 1984):

$$\gamma_H^T = \gamma_H^F \Big/ \left(1 + \frac{[SO_4^{2-}]}{K^*_{SO4}|X_0}\right) \quad \text{(eq. S8)}$$

where γ^F_H is the activity coefficient of free hydrogen ion as calculated from the specific interaction model, the total concentration of sulfate [SO_4^{2-}] scales proportionally with salinity as in modern seawater, and $K_{SO4}^*|X_0$ is the empirical conditional equilibrium constant for hydrogen-sulfate deprotonation in modern seawater of Dickson (1990a).

Text S4.

Model verification

We ascertain the skill of our simplified implementation of the MIAMI model in two ways: (1) the [Ca^{2+}] and [Mg^{2+}] sensitivity of our model implementation are compared against the original MP98 MIAMI model (Figure S1), and (2) the raw model predicted equilibrium constants (e.g., $pK^*_{MyAMI}(T, S, X_0)$ term in equation S2) are compared against the empirical equilibrium constants over a wide range of temperature and salinity (Figure 2 and S2). The first test shows that our MyAMI model implementation is congruent to the original MP98 MIAMI, whereas the second test demonstrates that the Pitzer-type modeling approach taken by the MIAMI-class models can predict empirical equilibrium constants typically to within a few percent over a wide range of temperature and salinity (at modern seawater composition X_0). Notwithstanding the modest residual deviations, the agreement between MyAMI predicted and empirical equilibrium constants (Figure 2 and S2) suggests that MyAMI must at least have skill to predict the sensitivities of the equilibrium constants to [Ca^{2+}] and [Mg^{2+}] change. In this context, we are confident in our approach of using the model-predicted sensitivities in conjunction with the empirical equilibrium constants (equation S2a and S2b).

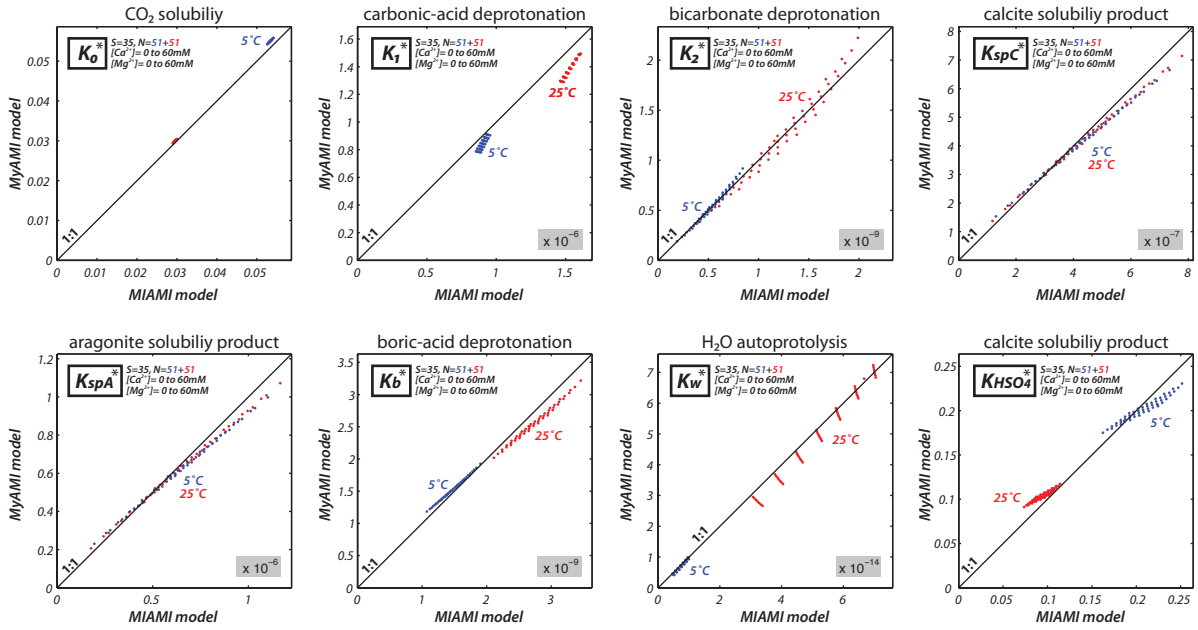

Figure S1. The MIAMI model (Millero and Pierrot, 1998) and our new derivative MyAMI model agree well overall. Residual differences are in large part due to different choice of thermodynamic data (see Table 2).

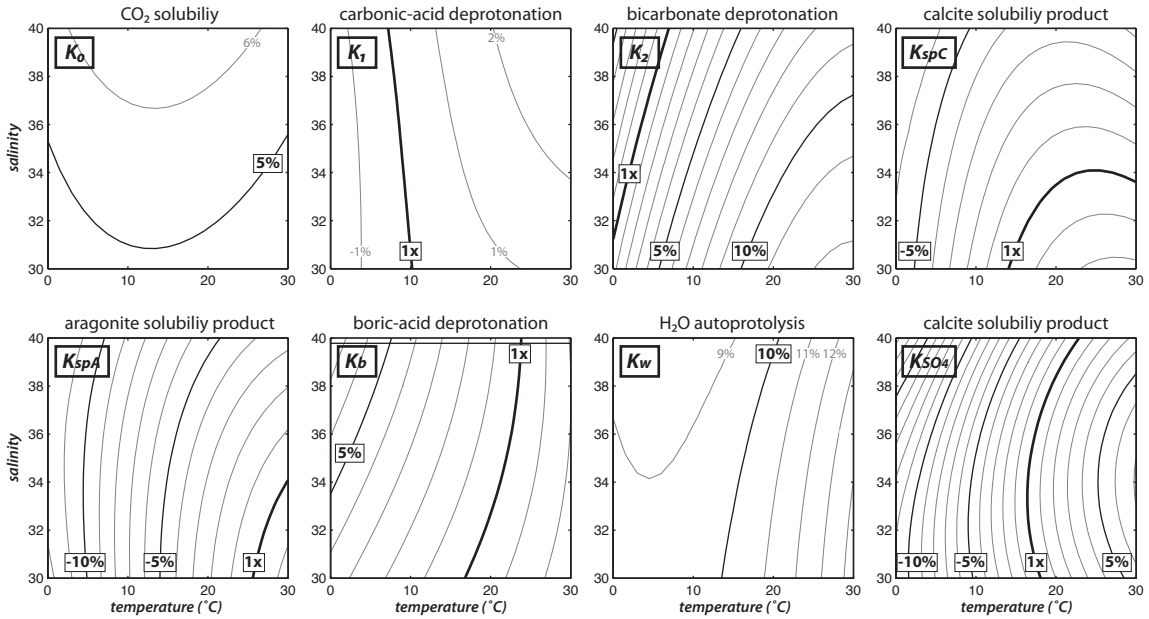

Figure S2. Comparison for modern seawater of experimentally determined "empirical" equilibrium constants (see Dickson et al., 2007) and raw MyAMI calculated equilibrium constants (i.e., before removing the deviation according to equation 2). The deviation of the equilibrium constants (ΔK*) is shown in percent, with positive values indicating that empirical K* is greater than calculated K*. The empirical equilibrium constants are taken from: (K_0*) Weiss, 1974; (K_1* and K_2*) Luecker et al., 2000; (KB*) Dickson, 1990b; (KHSO4*) Dickson, 1990a; (KspC*and KspA*) Mucci, 1983; and (Kw*) Millero, 1995. The thermodynamic equilibrium constants used to calculate conditional equilibrium constants are taken from: (K_0 and K_1) Plummer and Busenberg, 1982; (K_2) Harned and Scholes, 1941 refit by Millero, 1979b; (KB) Owen, 1934, Manov et al., 1944 refit by Millero, 1979b; (KHSO4) Campbell et al., 1993; (KspC and KspA) Mucci, 1983; and (Kw) Harned and Owen, 1958 refit by Millero, 1979b. All conditional constants are on the total pH scale calculated using KHSO4* of Dickson (1990a).

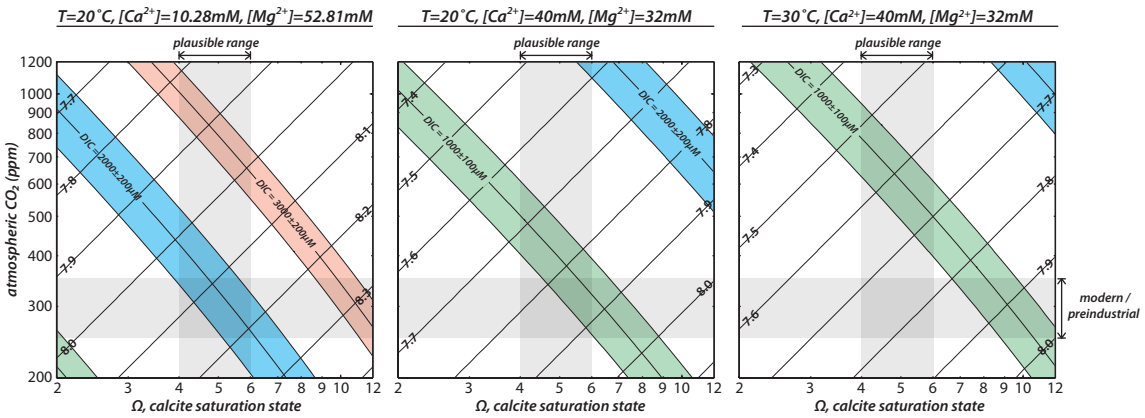

Figure S3. Thermodynamic Ω-CO_2-DIC-pH relationship for three cases of major ion composition and temperature that represent: (left) modern seawater composition at 20˚C, (center) scenario for Cretaceous seawater composition at 20˚C, and (right) scenario for Cretaceous seawater composition at 30˚C. Salinity (and ionic strength) is held constant at 35. Equilibrium constants are used according to equations 10 and 11. Blue, red and green shading represents DIC ranges from 1800-2200µM, 2800-3200µM and 900-1100µM, respectively. Gray shading indicates modern and Eocene target CO_2 levels and the plausible rage of calcite Ω. The very mild curvature of the DIC contours results from the log(DIC/HCO_3^-) term in equation 11. Contours of ALK would run almost parallel to DIC contours so as to yield: (1) DIC addition at constant ALK shift the acid/base chemistry up and left in this plot (almost following DIC contours), and (2) ALK addition at constant DIC shift the acid/base chemistry down and right in this plot (along DIC contours). Figure 4 in the main manuscript shows the same experiments but for the Eocene seawater scenario instead of the Cretaceous scenario.

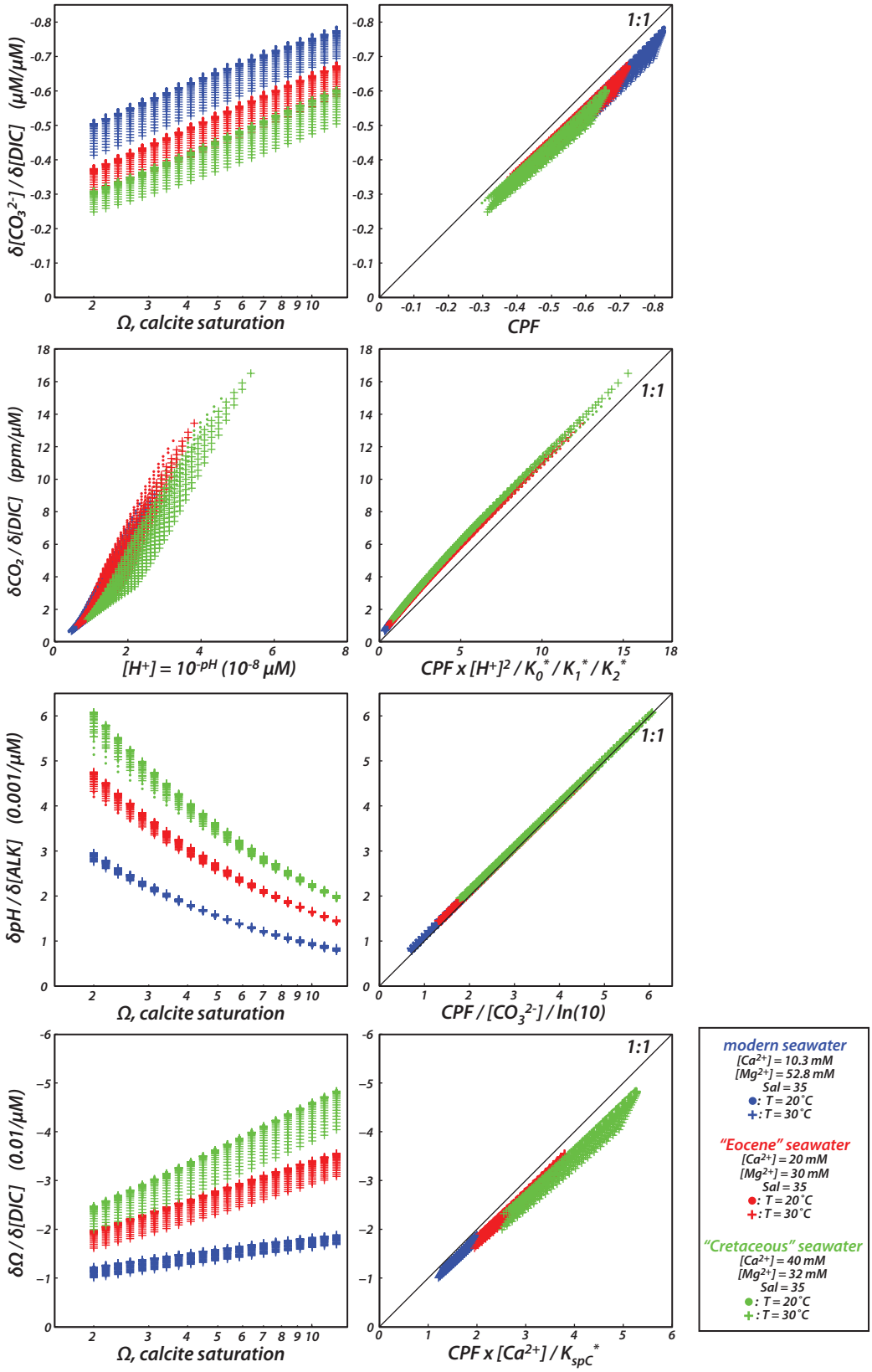

Figure S4. Sensitivity of $[CO_3^{2-}]$, pH, Ω and CO_2 to incremental DIC and ALK change (δ/δDIC and δ/δDIC, respectively) under three cases: (blue) modern seawater major ion composition, (red) "Eocene" scenario major ion composition, and (green) "Cretaceous" scenario major ion composition. In all cases, salinity is 35, and (circles) T=20˚C or (plus symbols) T=30˚C. The symbols of each color span the entire solution space of CO_2 = 200ppm to 1200ppm and Ω = 2 to 12. The sensitivity factors (i.e., inverse buffer factors) are numerically determined by perturbing DIC or ALK by 0.1μM. The panels on the right hand side compare numerically determined sensitivity factors (y-axis) against the approximate analytical solution shown in equation 12.